Small signal stability analysis of proportional resonant controlled VSCs connected to AC grids with variable X/R characteristic

by

Marta Haro Larrode

A thesis presented for the degree of
Doctor of Philosophy

Department of Electrical Engineering
University of the Basque Country
Spain
March 2020

Inter-University Doctoral Programme in Electrical Energy Systems

The author would like to express her gratitude to the international PhD thesis reviewers for accepting to evaluate this work.

- Carlos Ugalde Loo, Reader in Electrical Power Systems in Cardiff University, United Kingdom.
- Salvatore D'Arco, Senior Scientist from the Department of Energy Systems, SINTEF Energy Research, Norway.

The author gratefully acknowledges to TECNALIA Research Centre for its support for the achievement of the objectives of this PhD dissertation.

Acknowledgements

First and foremost, I would like to express my deep gratitude to my supervisors Dr. Pablo Eguia and Dr. Maider Santos for their supervision, continuous support and engagement along with the PhD thesis. I have been very fortunate to find such a dedicated energy, encouragement and enthusiasm in my supervisors. I would like also to give many thanks to Dr. Salvador Ceballos for his remarks whenever guidance was needed, and to Dr. Agurtzane Etxegarai for her valuable collaboration in the initial stage of the PhD thesis.

With regard to Tecnalia staff, I would also like to acknowledge Asier Gil and Raúl Rodriguez for their help when I came across the greatest technical difficulties in the thesis. Thanks to all the workforce in Tecnalia for the intriguing environment of innovative ideas to make my experience productive and stimulating. I humbly thank my fellow PhD candidates, Andrés, Izar, Alize, Diego and Ibon for their nice and friendly environment I have had during this period.

As for my stay in NTNU, Trondheim, I feel grateful for the help of Professor Elisabetta Tedeschi and Dr.Gilbert Bergna, in adding new perspectives and modelling aspects of modular multilevel converters in the last stage of the research period. And I would like also to thank my colleagues at NTNU, Nam, Spyridon, Daniele, Ole, Andreas, Danilo, Aravinda, Damiano, Erick and Augusto for the great companionship.

I would also like to thank my friends, my family, my flatmates and my cats for their love, encouragement, understanding and support.

March 2020, Bilbao

Marta Haro Larrode

Preface

This thesis is submitted to the University of the Basque Country (UPV) in partial satisfaction of the requirements for the degree Doctor of Philosophy. The present thesis has been developed at Tecnalia Research Innovation in Derio (Spain) and at the Department of Electrical Engineering of the University of the Basque Country (UPV-EHU) in Bilbao (Spain). The PhD thesis has been conducted in the period from March 2016 to December 2019 with Dr.Pablo Eguia and Dr. Maider Santos as supervisors. In 2019, the author moved to the Norwegian University of Science and Technology (NTNU) at the department of Electrical Engineering for an international research stay, where a collaborative work was developed with Professor Elisabetta Tedeschi and Dr Gilbert Bergna.

This work is part of the activities in the HVDC Link and Road2DC projects.

The HVDC Link project, *HVDC links for marine energy evacuation: future solution*, funded by Basque Government, has been a collaboration between Tecnalia, the University of the Basque Country, Arteche and Ormazábal. Within this project, a simulation and an experimental platform have been developed which represents the complete marine energy system connected to the AC grid though a point-to-point HVDC link. In this PhD thesis, the control strategies of such system and interaction with AC grid control layers have been validated via simulations in DIgSILENT PowerFactory.

The Road2DC project, *New Tools for the Design and Control of Hybrid AC/DC Distribution*, funded by Basque Government, has been focused on settling the necessary technical and scientific basis through the development of mathematical and control tools to demonstrate the applicability of hybrid AC/DC grids from the perspective of efficiency and reliability, allowing the industrial network of the Basque Country to design and develop solutions for the future electrical grids. In order to achieve the mentioned objective, different agents have formed a Road2DC consortium, namely: the Polytechnic School of Mondragon Unibertsitatea, the technological Institute of Deusto Foundation of the University of Deusto, Tecnalia Research & Innovation, IK4-IKERLAN and the R&D Company unit of Ingeteam R&D Europe, S.L. The main research paper of this PhD thesis has been in line with the Road2DC project objective.

In addition, this research work is of high interest for Tecnalia in the aim of being experts in instability issues of renewable energy systems.

Abstract

With the massive integration of renewable energy sources in the AC networks, the AC grids are becoming weaker and weaker, more complex and chaotic. Phenomena such as the disconnection of AC lines, trip of converters or load variations produced by the intermittent nature of renewable generation, are starting to provoke changes in the impedance and inductive-resistive characteristic values of even the stiff AC networks. As long as the AC network is weakened, its equivalent impedance increases and this derives into undesired changes in the active and reactive power magnitudes, which imply sudden voltage variations at different points of the AC grid. Alongside with it, this also causes the possible deterioration of converters and the worsening of power quality. A partial solution to this issue is to curtail power where it is generated, but at the cost of increasing local losses. Another solution is to improve the robustness of converter's control to make them able to cope with these increasingly frequent scenarios.

Voltage source converters, and especially modular multilevel converters, present a set of features which make them ideal for this type of scenarios as they have a better dynamic performance compared to current source converters, since they operate at a higher switching frequency. Besides, voltage source converters present low-voltage ride through capabilities and decoupled control of active and reactive power, which makes them able to cope with undesired changes in the balance of active and reactive power.

The inner control schemes of a voltage source converter have been implemented generally by means of proportional integral controllers, although they produce errors in steady-state regime, do not manage events in unbalanced load-flow and their implementation requires decoupling the dependency in three-phase systems. Within the last decade, proportional resonant controllers have appeared as an alternative to proportional integral controllers, since they allow the handling of balanced and unbalanced operation and the removal of the phase-locked loop and Park transforms.

Different methodologies have been developed for the control of voltage source converters, generally governed by proportional integral controllers, under scenarios such as the progressive reduction of the strength of the AC grid to which they are connected. However, very few studies have been carried out on voltage source converters controlled by proportional resonant schemes, where the AC grid is weakened progressively. And still less where the variations of the inductive-resistive characteristic of the AC grid have been considered in such scenario.

Above all, no study has determined the minimum percent variation of X/R ratio that could drive the system to instability, even when their proportional resonant controllers have been designed for weak AC grid ranges.

In this PhD thesis, a methodology is proposed to tune the proportional resonant controller of a voltage source converter connected to an AC grid with variable strength and X/R ratio. Such methodology is based on two formulations to study the small signal stability of the system: the state-space system representation and the system's eigenvalues trajectories. By means of the state-space representation, a small signal model of the system under study is constructed. Once constructed, the small signal model is validated with simulations in DIgSILENT PF. The methodology uses the trajectories of eigenvalues of the small signal model to characterise the small signal stability of the system. This process is carried out, on the one hand, by considering the variability of the AC grid stiffness while the X/R ratio is constant and, on the other hand, while the X/R ratio varies. In each stage, ranges of PR k_p and k_i values which ensure stability are obtained, as well as other ranges which cannot maintain it. However, the results of this PhD thesis demonstrate that a small deviation of 20% in the X/R ratio drives the system to instability. In such cases, the methodology proposes two new tuning strategies for PR controller to return the system to the stable region when the AC grid is weak, and its X/R ratio has been slightly modified.

Finally, several electromagnetic transient (EMT) simulation results in DIgSILENT PF verify both stable and unstable cases and the new tuning strategies proposed by the methodology. Besides, the methodology, analysis, cases and new tuning strategies have been justified to be extended for modular multilevel converter topologies, under the compensated modulation approach.

Resumen

Con la creciente integración de las energías renovables, las redes eléctricas AC se están volviendo cada vez más débiles, más complejas y caóticas. Fenómenos como la desconexión de líneas AC, el bloqueo de convertidores, o variaciones de carga debidas a las intermitencias de la generación renovable, están comenzando a producir cambios en los valores de impedancia y en las características inductivo-resistivas de incluso las redes fuertes. Conforme una red AC se debilita su impedancia equivalente aumenta, y esto provoca cambios indeseados en las magnitudes de potencia activa y reactiva, que derivan en variaciones repentinas de tensión en diferentes puntos de la red AC. Esto también conlleva el deterioro de los convertidores y empeoramiento de la calidad de onda. Una solución parcial a este problema es limitar la potencia allí donde se genera, en perjuicio de aumentar las pérdidas locales. Otra solución es introducir controles de convertidores más robustos, para que sean capaces de sortear estos escenarios cada vez más frecuentes.

Los convertidores de fuente de tensión, y en especial los convertidores modulares multinivel, presentan una serie de prestaciones que los hacen idóneos para esta clase de escenarios, dado su mejor comportamiento dinámico frente a los convertidores de fuente de corriente, al operar a una frecuencia de conmutación mayor. Además, los convertidores de fuente de tensión disponen de capacidades LVRT y control desacoplado de potencia activa y reactiva, lo que les hace resilientes frente a cambios indeseados en el balance de potencia activa y reactiva.

Los controles internos de los convertidores de fuente de tensión se han implementado generalmente por medio de controladores proporcional integrales, a pesar de que producen errores en régimen estacionario, no operan en régimen de flujo desequilibrado y su implementación requiere desacoplar su dependencia de fase en sistemas trifásicos. En la última década, los controladores proporcional resonantes han aparecido como alternativa a los proporcional integrales, debido a su capacidad de manejar operación tanto equilibrada como desequilibrada y a que eliminan la necesidad de utilizar un phase-locked loop y las transformadas de Park.

Se han desarrollado diversas metodologías para el control de convertidores de fuente de tensión, generalmente mediante controladores proporcionales integrales, en escenarios como la reducción progresiva de la fortaleza de la red AC a la que están conectados. Sin embargo, muy pocos estudios se han realizado con convertidores de fuente de tensión gobernados por controladores proporcional

resonantes, donde la red AC sea progresivamente más débil. Tampoco se han considerado en dicho escenario variaciones de la característica inductivo-resistiva de la red AC. Y sobre todo, qué variación mínima porcentual del ratio X/R podría desestabilizar el sistema, aún cuando su control se haya diseñado para los rangos de red AC débil.

En esta tesis doctoral se propone una metodología de parametrización del control proporcional resonante de un convertidor de fuente de tensión conectado a una red AC con fortaleza y característica inductivo-resistiva variables. Dicha metodología se basa en dos formulaciones para el estudio de la estabilidad de pequeña señal: la representación del espacio de estados y las trayectorias de los autovalores del sistema. Con la representación del espacio de estados se ha construido un modelo de pequeña señal. Una vez construido se ha validado con simulaciones EMT en DIgSILENT PF. La metodología usa la trayectoria de los autovalores del modelo de pequeña señal para caracterizar la estabilidad de pequeña señal del sistema objeto de estudio. Este proceso se ha efectuado, por un lado, considerando una fortaleza variable de red AC mientras el ratio X/R es constante, y por otro, mientras el ratio X/R varía. En cada una de las dos etapas se han obtenido rangos de valores k_p y k_i del controlador PR que aseguran la estabilidad y otros que no la pueden mantener. Sin embargo, los resultados de esta tesis demuestran que tan solo una desviación del 20% en el ratio X/R con respecto a su valor habitual puede hacer perder al sistema su estabilidad en pequeña señal cuando la red AC es débil. En tales casos, la metodología propone dos nuevas estrategias de parametrización del control proporcional resonante para devolver el sistema a la estabilidad cuando la red AC es débil y su ratio X/R se ha modificado levemente.

Finalmente, se han obtenido distintos resultados de simulación EMT en DIgSILENT PF que han permitido verificar los casos tanto estables como inestables y las estrategias de parametrización propuestas por la metodología. Además, se ha justificado la extensión de la metodología para la topología de convertidor modular multinivel bajo la hipótesis de modulación compensada.

Laburpena

Korronte alternoko sareak gero eta ahulagoak, konplexuagoak eta kaotikoagoak bilakatzen ari dira, energia iturri berriztagarrien integrazio masiboa dela eta. Korronte alternoko lineen deskonexioak, bihurgailuen desarratzeak edota iturri berriztagarrien aldakortasunaren ondoriozko karga-aldaketak sareetako inpedantzia eta ezaugarri induktibo-erresistiboetan aldakuntzak eragiten ari dira, baita sare sendoetan ere. Korronte alternoko sarea ahultzen doan einean, haren inpedantzia baliokidea handitzen da eta horrenbestez, potentzia aktiboaren eta erreaktiboaren magnitudeetan aldaketa kaltegarriak sortzen dira. Hala, tentsioak bat-bateko gorabeherak jasan ditzake sarearen puntu ezberdinetan. Ondorioz, bihurgailuak honda daitezke eta hornidura elektrikoaren kalitateak okerrera egin dezake. Konponbide posible bat tokiko potentzia-sorkuntza mugatzea da, baina galerak eragitearen truke. Gero eta ohikoagoak diren egoera horiei aurre egiteko beste irtenbide bat bihurgailuen kontrol-algoritmoen sendotasuna hobetzea da.

Tentsio-iturriko bihurgailuek (ingelesez VSC) eta bereziki maila anitzeko bihurgailuek (ingelesez MMC) jardunbide dinamiko hobea dute korronte-iturriko bihurgailuekin (ingelesez CSC) alderatuz gero, kommutazio-maiztasun handiagora lan egiten baitute. Gainera, VSCek tentsio-hutsei aurre egiteko ahalmena (ingelesez LVRT) aurkezten dute eta potentzia aktiboaren eta erreaktiboaren kontrol banandua dute. Hala, potentzia aktiboaren eta erreaktiboaren fluxuetan sortutako nahiezeko aldakuntzak menderatzeko gai dira eta sare ahuletako egoera berriak gainditu gai izan daitezke.

Orokorrean, VSCen barne-kontrol eskemak kontrolagailu proportzional-integralen (PI) bidez gauzatzen dira, hainbat desabantaila izan arren. Izan ere, erregimen iraunkorrean erroreak sortzen dituzte, karga-fluxu desorekatuetako gertaerei ezin diete aurre egin eta sistema trifasikoetako fase-menpekotasuna banantzea eskatzen dute. Azken hamarkadan, ordea, kontrolagailu proportzional erresonanteen (PR) erabilerak goraka egin du PI motako kontrolagailuekiko alternatiba bezala, operazio orekatua eta desorekatua baimentzen duelako eta faseko blokeo-begizta (ingelesez PLL) zein Park-en transformatua ere ekiditen direlako.

VSCak kontrolatzeko hainbat metodologia garatu dira, orokorrean PI motako kontrolagailuen bitartez eta konektatu beharreko sare alternoen etengabeko sendotasun -galera egoerak gogoan hartuz. Hala ere, ikerlan gutxi garatu dira PR motako kontrolagailuei buruz sistema elektrikoen pixkanakako ahultasuna aintzat hartuz. Eta are eta gutxiago dira sare elektriko alternoen ezaugarri induktibo-erresistiboak aztertu dituzten ikerketak. Baina batez ere, PR motako

kontrolagailuak sare elektriko ahuletarako propio diseinatu arren, orain artean ez da zehaztu sistema desengokortasunera bidera lezakeen X/R proportzioaren gutxieneko ehuneko aldakuntza.

Honako doktoretza-tesian, sendotasun eta X/R proportzio aldakorreko sare elektriko ahuletan konektatutako VSCen PR kontrolagailuak doitzeko metodologia proposatzen da. Metodologia hori bi adierazpenetan oinarritu da sistemaren seinale txikiko egonkortasuna ikasteko: egoera-espazio sistemen adierazpidea eta sistemaren balio propioen ibilbideak. Egoera-espazioen adierazpidearen bitartez, aztertu beharreko sistemaren seinale txikiko eredu bat gauzatu da eta ondoren, DIgSILENT PF tresnaren bitartez burututako simulazioekin egiaztatu da eredua. Metodologiak seinale txikiko ereduaren balio propioen ibilbideak erabili ditu sistemaren seinale txikiko egonkortasuna karakteriza ahal izateko. Prozedura hori bi ikuspuntutik burutu da: alde batetik, sare alternoaren sendotasuna aldatuz baina X/R proportzioa konstante mantenduz eta bestalde, X/R proportzioa aldaraziz. Pauso bakoitzean egonkortasuna bermatzen duten PR kontrolagailuaren kp eta ki balioak lortu dira, baita desegonkortasuna eragiten duten tarteko balioak ere. Izan ere, honako doktoretza-tesiaren emaitzek X/R proportzioaren %20ko desbiderapen txikiek sistema desegonkortasunera bidera dezaketela frogatu dute. Kasu horietarako, proposatutako metodologiak PR kontrolagailuentzako bi doitze-estrategia berri aurkezten ditu sistema zonalde egonkorrera bueltarazteko sare elektriko alternoa ahula denean eta X/R proportzioa arinki aldatu denean.

Azkenik, DIgSILENT PF tresnaren bitartez burututako EMT simulazioekin kasu egonkor eta ez-egonkorrak egiaztatu dira, baita metodologiak proposatutako doitze-estrategia berriak ere. Gainera, metodologia, analisia, ikasketa-kasuak eta doitze-estrategia berriak MMC topologietara zabaldu dira, modulazio konpentsatuaren hurbiltzea erabiliz.

Contents

Acknowledgements **i**

Preface **iii**

Abstract **v**

Resumen **viii**

Laburpena **xi**

Contents **xiv**

List of Figures **xix**

List of Tables **xxvii**

Nomenclature **xxix**

Glossary **xxxviii**

1 Introduction **1**

1.1 Context and motivation 1

1.1.1 HVDC-HVAC systems 1

1.1.2 Stability of HVDC-AC systems [9] 4

1.2 Problem statement and research questions 6

1.2.1 Current controllers in VSCs connected to AC systems . . . 6

1.2.2 Analytical methods to study the small signal interaction between VSCs and AC grids 8

1.2.3 Small signal interactions between VSC converters and AC grids 11

1.3 Scope of the thesis 12

1.4 Main contributions of the thesis 13

1.5 List of publications 14

1.6 Outline of the thesis 15

2 Voltage source converters in a weak AC grid environment **18**

2.1 Introduction 18

2.2 Topologies for power converters for medium- and high-voltage power system 18

2.2.1 Cycloconverter . . . 18
2.2.2 Current source converter . . . 19
2.2.3 Voltage source converters . . . 20
2.3 Challenges and drivers of VSCs in the context of weak grids with varying X/R characteristic . . . 20
2.3.1 The importance of the AC system stiffness . . . 22
2.3.2 The importance of X/R ratio . . . 26
2.4 Grid code requirements . . . 28
2.4.1 Active power/frequency response . . . 28
2.4.2 Reactive power/voltage response . . . 32
2.4.3 Low-voltage ride through response . . . 34
2.4.4 Recent modifications of the grid code . . . 35
2.5 Control systems for VSC . . . 36
2.5.1 Control at MTDC grid level . . . 36
2.5.2 VSC outer control level . . . 43
2.5.3 VSC inner current control level . . . 49
2.6 Types of proportional resonant controllers . . . 54
2.7 An especial case: modular multilevel converters . . . 64
2.8 Small signal interactions between VSCs and AC grids in an HVDC environment . . . 70
2.8.1 General characterisation of interactions, approaches and simplifications [34, 35] . . . 70
2.8.2 Impact of dynamic interactions introduced by VSC control parameters . . . 74
2.8.3 Impact of dynamic interactions introduced by the change in AC grid characteristics . . . 79
2.9 Research gaps . . . 84
2.10 Summary . . . 84

3 Novel methodology for interaction analysis between a VSC and an AC grid 87
3.1 Introduction . . . 87
3.2 Description of the methodology . . . 87
3.3 Small signal model . . . 89
3.3.1 Outer loop controller . . . 90
3.3.2 Inner loop controller: proportional resonant current controller . . . 92
3.3.3 VSC with modulation interface . . . 94

3.3.4 VSC output filter and AC line . . . 96
3.4 Compensated modulation approach . . . 97
3.5 Summary . . . 101

4 Application Case **103**
4.1 Introduction . . . 103
4.2 Part I: Numerical validation of the small signal model . . . 103
4.2.1 Application to a case study . . . 103
4.2.2 Preliminary tests . . . 105
4.2.3 Justification of the main control parameters . . . 116
4.2.4 Closed-loop numerical validation of small signal model . . . 117
4.3 Part II: Eigenvalue trajectory analysis . . . 119
4.3.1 Presentation of case studies . . . 120
4.3.2 Eigenvalue trajectory analysis with constant X/R characteristic . . . 122
4.3.3 Eigenvalue trajectory analysis with variable X/R characteristic . . . 124
4.4 Implications of the methodology for tuning PR controllers . . . 129
4.4.1 Participation factor analysis . . . 129
4.4.2 Final remarks . . . 131
4.5 Summary . . . 133

5 Verification of the methodology **135**
5.1 Introduction . . . 135
5.2 Model used for the verification of the methodology . . . 135
5.3 Verification of cases with constant X/R characteristic . . . 135
5.4 Verification of cases with variable X/R characteristic . . . 140
5.5 Verification of solutions to an unstable case . . . 145
5.6 Justification of the methodological process . . . 148
5.7 Summary . . . 149

6 Conclusions and future work **151**
6.1 Conclusions . . . 151
6.2 Future work . . . 155

Appendix A- Analytical methods for stability analysis **157**

Appendix B- EMT model parameters in DIgSILENT PF **170**

Appendix C- Parameters of the small signal model **177**

References **179**

List of Figures

1 HVDC projects at worldwide scale [1]. 2
2 Definition of transient stability [9]. 4
3 Classification of small signal stability [26, 27]. 8
4 Single-infeed system composed by an HVDC station connected to an AC grid, defined by Z_s and E [62]. 23
5 Multiple-infeed system composed by several HVDC stations connected to different AC grids, defined by Z_s and E [62]. 23
6 POC voltage behaviour in response to (a)SCR and X/R ratio variations and (b)in-feed power and grid parameters change [36]. . . . 27
7 Reactive power and power factor regulation for ±5% POC voltage deviation at SCR=2 (a)SCR and X/R ratio variations and (b)in-feed power and grid parameters change [36]. 27
8 Minimum Active Power reduction in Rectifier Mode for LFSM [75]. 29
9 Minimum Active Power reduction in Rectifier Mode for FSM [75]. 30
10 Frequency ranges of operation in different countries [14]. 31
11 Voltage control according to UK national grid code [75]. 32
12 Minimum transient voltage response [75]. 34
13 Low Voltage Ride Through curves for different countries [14]. . . . 35
14 Most common arrangements for HVDC grids composed by VSC [42]. 37
15 Primary, secondary and tertiary control concepts [80]. 38
16 Comparison of primary, secondary and tertiary control in AC and DC networks [80]. 39
17 Basic VP characteristics for MTDC control (a) Slack bus, (b) Voltage margin, (c) VP droop, (d) VP droop with deadband. 40
18 HVDC grid with Master-Slave Control [85]. 41
19 Control scheme of a VSC terminal connected to an active grid [91]. 44
20 VdcQ control scheme of a VSC terminal connected to an active grid: calculation of d current reference 45
21 VdcQ Control scheme of a VSC terminal connected to an active grid: calculation of q current reference 46
22 PQ Control scheme of a VSC terminal connected to an active grid: calculation of d current reference 46
23 Control scheme for a VSC terminal connected to a passive grid . 47
24 Inner current control scheme based on PI controllers [16]. 50

25 Single-phase equivalent representations of PR and synchronous PI controllers [23]. 51
26 Open loop Bode diagram for PI controller. 52
27 Open loop Bode diagram for PR controller. 53
28 General classification of PR Controllers according to [25, 100, 101]. 55
29 Closed loop frequency response of the inner control loop with ideal PR controller and with voltage decoupling branch [100]. 56
30 Closed loop frequency response of the inner control loop with non-ideal PR controller and with voltage decoupling branch [100]. . . . 57
31 Closed loop frequency response of the inner control loop with complex vector PR controller and with voltage decoupling branch [100]. 57
32 The PR-based controller: (a) PR, (b) PRXF, (c) PRXC and (d) PRX2 [101]. 59
33 Bode plot of open-loop (blue) and closed-loop(red) PR controller [101]. 60
34 Bode plot of open-loop (blue) and closed-loop(red) PRXF controller [101]. 61
35 Bode plot of open-loop (blue) and closed-loop(red) PRXC controller [101]. 61
36 Bode plot of open-loop (blue) and closed-loop(red) PRX2 controller [101]. 62
37 The proposed modification of PRX2 [101]. 63
38 Topology of a three-phase MMC [98]. 65
39 Leg of an MMC [38]. 67
40 Overview of configuration and control system for a single-terminal MMC [38]. 70
41 Configuration of an AC power system integrated with a VSC-based HVDC line [34, 35]. 71
42 Configuration of an AC power system integrated with a VSC-based MTDC grid [34, 35]. 72
43 Multi-infeed VSCs/AC power system [34, 35]. 73
44 MTDC power system with multi-independent AC power systems [34, 35]. 73
45 Eigenvalue trajectory analysis when the active damping gain $k_{AD,dc}$ is varied from 0 to 100 [104]. 75
46 DC Grid Test System proposed by Cigré [105]. 75
47 Eigenvalue trajectory analysis when $R_{v,dc}$ is varied from 0 to 40 [105]. 76

48 Eigenvalue trajectory analysis of an MMC-based HVDC link when the DC voltage controller response time is varied from 1ms to 1 s [78]. 77
49 New England 39-bus system with four-terminals VSC stations [106]. 77
50 The dynamic behaviour of DC voltage (a) DC voltage in VSC1, (b) DC voltage in VSC2, (c) DC voltage in VSC3 and (d) DC voltage in VSC4. [106]. 78
51 Amplitude of AC voltage at the PCC of VSC1 for (a) PI-1 and (b) PI-2 and DC voltage of VSC1 for (c) PI-1 and (d) PI-2 [106]. . 79
52 Two-terminal VSC system under study [20]. 80
53 Pole placement for the direction of power from VSC1(O) to VSC2, starting at O and ending at Δ when: (a) VSC1 is connected to a strong AC grid and (b) VSC1 is connected to a weak AC grid [20]. 81
54 Nyquist contours (a): Solid, DVC gain set to 9.23 and power flow set to 0.5 p.u.; dashed, DVC gain set to 9.23 and power flow set to 0.4 p.u. and (b) Solid: DVC gain set to 9.23 and power flow set to 0.5 p.u.; dashed, DVC gain set to 4.61 and power flow set to 0.5 p.u. [20]. 81
55 Trajectory of eigenvalues for a reduction in SCR (20 to 1) in the MTDC grid under study for (a) Predictive control strategy and (b) PID control [107]. 82
56 Hybrid LCC-VSC system under study [108]. 83
57 Eigenvalue trajectory analysis when the lie line length is varied between 10 to 100 km for AC1 and AC2 grid strength set to 1.2 [108]. 83
58 Diagram of the proposed methodology. 88
59 VSC-AC system schematics 90
60 Scheme for outer loop controller 91
61 Proportional-Resonant Scheme for inner loop controller in $\alpha\beta$ frame 92
62 Proportional-Resonant Scheme for inner loop controller in dq frame 93
63 Normalization block and VSC converter in: (a) non-linearised version and (b) linearised version 95
64 Π-Equivalent model for AC line 96
65 Stored energy, W (p.u.) for uCM control. 98
66 Circulating current, $i_{S,z}$ (p.u.) for uCM control. 98
67 Grid dq currents, i_d (p.u.), i_q (p.u.) for uCM control. 98
68 Stored energy, W (p.u.) for CM control. 99
69 Circulating current, $i_{S,z}$ (p.u.) for CM control 99

70 Grid dq currents, i_d (p.u.), i_q (p.u.) for CM control. 100
71 Schematic of the P2P HVDC link 104
72 DC Voltage/Active Power during changes in offshore generation. . 105
73 AC Voltage/Reactive power during changes in offshore generation 106
74 AC voltage/Reactive Power during AC voltage variations applied at the onshore AC grid. 107
75 DC Voltage/Active Power during AC voltage variations applied at the onshore AC grid. 108
76 AC voltage /Reactive Power during the three-phase short-circuit of 140 ms duration and Xcc=0.450hms. 109
77 DC Voltage/Active Power during the short-circuit of 140 ms and Xcc=0.45 Ω 110
78 AC voltage/Reactive Power during the three-phase short-circuit of 1.2 s duration and Xcc=11 Ω. 111
79 DC Voltage/Active Power during the short-circuit of 1.2 s and Xcc=ll Ω. 112
80 DC Voltage/Active Power during the short-circuit of 1.2 s and Xcc=0.45 Ω with and without brake resistance. 113
81 DC voltage/Active Power during two-phase short-circuit applied at the onshore AC grid according to the control option. 114
82 Onshore terminal currents during two-phase short-circuit applied at the onshore AC grid. 115
83 Bode diagram of PR controller tuned at k_p=1.5 and k_i=30000. . . 116
84 DC voltage response under a perturbation in DC voltage setpoint. 117
85 Small signal model validation under a perturbation in DC voltage reference: $I_{d,ref}$ (p.u.) and $I_{q,ref}$ (p.u.). 118
86 Small signal model validation under a perturbation in AC voltage reference: $V_{d,ref}$ (p.u.) and $V_{q,ref}$ (p.u.). 118
87 Small signal model validation under a perturbation in AC voltage reference: $V_{d,ref}$ (p.u.) and $V_{q,ref}$ (p.u.). 119
88 Simplified system under study. 120
89 Trajectory of eigenvalues in a stiff AC grid (SCR=25) when PR controller parameters are varied: (a) k_p between 3 and 0.1 while k_i=30000 and (b) k_i between 5000 and 50000 while k_p=1.5. 123
90 Trajectory of eigenvalues in a weak AC grid (SCR=2.3) when PR controller parameters are varied: (a) k_p between 3 and 0.1 while k_i=30000 and (b) k_i between 5000 and 50000 while k_p=1.5. 123

91 Trajectory of eigenvalues in an AC grid with X/R=8.37 whose strength is varied from a stiff (SCR=25) to a weak (SCR=2.3) case, when PR controller parameters are set to (a) k_i=30000 and k_p=1.5 and (b) zoomed image of (a). 124
92 Trajectory of eigenvalues in a weak AC grid (SCR=2.3) when PR controller parameters are set to k_i=30000 and k_p=1.5, and the X/R ratio is varied by a: (a) -20% (X/R=6.61), (b) -10% (X/R=7.5), (c) +10% (X/R=9.2) and (d) +20% (X/R=10) from its usual value. 126
93 Displacement of the critical eigenvalue when the X/R characteristic deviates from -20% (X/R=6.61) to +20% (X/R=10). 127
94 Solution for the unstable case based on the modification of k_p (a) in a weak AC grid (SCR=2.3) case, when k_i=30000 and k_p is varied from k_p=1.5 to k_p=1.65 and (b) zoomed image of (a). . . . 127
95 Solution for the unstable case based on the modification of k_i (a) in a weak AC grid (SCR=2.3) case, when k_p=1.5 and k_{ip} is varied from k_p=30000 to k_p=250000 and (b) zoomed image of (a). 128
96 Participation shares of state variables on eigenvalues λ_{11} and λ_{12} of Table 4. 130
97 Verification of a stiff AC grid: (a) Module of AC voltage measured at the PCC ($V_{AC,PCC}$ (p.u.)) and AC voltage measured at the PCC in d coordinate ($V_{d,PCC}$ (p.u.)), (b) AC voltage measured at the PCC in q coordinate ($V_{q,PCC}$ (p.u.)), (c) Current reference for d coordinate ($I_{d,ref}$) and current measured at the PCC in d coordinate ($I_{d,PCC}$) and (d) Current reference for q coordinate ($I_{q,ref}$) and current measured at the PCC in q coordinate ($I_{q,PCC}$). 136
98 Verification of a stable case in a weak AC grid: (a) Module of AC voltage measured at the PCC ($V_{AC,PCC}$ (p.u.)) and AC voltage measured at the PCC in d coordinate ($V_{d,PCC}$ (p.u.)), (b) AC voltage measured at the PCC in q coordinate ($V_{q,PCC}$ (p.u.)), (c) Current reference for d coordinate ($I_{d,ref}$) and current measured at the PCC in d coordinate ($I_{d,PCC}$) and (d) Current reference for q coordinate ($I_{q,ref}$) and current measured at the PCC in q coordinate ($I_{q,PCC}$). 137

99 Verification of an unstable case in a weak AC grid for k_p=0.1 and k_p=30000: (a) Module of AC voltage measured at the PCC ($V_{AC,PCC}$ (p.u.)) and AC voltage measured at the PCC in d coordinate ($V_{d,PCC}$ (p.u.)), (b) AC voltage measured at the PCC in q coordinate ($V_{q,PCC}$ (p.u.)), (c) Current reference for d cooordinate ($I_{d,ref}$) and current measured at the PCC in d coordinate ($I_{d,PCC}$) and (d) Current reference for q cooordinate ($I_{q,ref}$) and current measured at the PCC in q coordinate ($I_{q,PCC}$). 139
100 Verification of an unstable case in a weak AC grid for a -20% variation of X/R: (a) Module of AC voltage measured at the PCC ($V_{AC,PCC}$ (p.u.)) and AC voltage measured at the PCC in d coordinate ($V_{d,PCC}$ (p.u.)), (b) AC voltage measured at the PCC in q coordinate ($V_{q,PCC}$ (p.u.)), (c) Current reference for d coordinate ($I_{d,ref}$) and current measured at the PCC in d coordinate ($I_{d,PCC}$) and (d) Current reference for q coordinate ($I_{q,ref}$) and current measured at the PCC in q coordinate ($I_{q,PCC}$). 141
101 Verification of an unstable case in a weak AC grid for a -10% variation of X/R: (a) Module of AC voltage measured at the PCC ($V_{AC,PCC}$ (p.u.)) and AC voltage measured at the PCC in d coordinate ($V_{d,PCC}$ (p.u.)), (b) AC voltage measured at the PCC in q coordinate ($V_{q,PCC}$ (p.u.)), (c) Current reference for d coordinate ($I_{d,ref}$) and current measured at the PCC in d coordinate ($I_{d,PCC}$) and (d) Current reference for q coordinate ($I_{q,ref}$) and current measured at the PCC in q coordinate ($I_{q,PCC}$). 142
102 Verification of a stable case in a weak AC grid for a +10% variation of X/R: (a) Module of AC voltage measured at the PCC ($V_{AC,PCC}$ (p.u.)) and AC voltage measured at the PCC in d coordinate ($V_{d,PCC}$ (p.u.)), (b) AC voltage measured at the PCC in q coordinate ($V_{q,PCC}$ (p.u.)), (c) Current reference for d coordinate ($I_{d,ref}$) and current measured at the PCC in d coordinate ($I_{d,PCC}$) and (d) Current reference for q coordinate ($I_{q,ref}$) and current measured at the PCC in q coordinate ($I_{q,PCC}$). 143

103 Verification of a stable case in a weak AC grid for +20% variation of X/R: (a) Module of AC voltage measured at the PCC ($V_{AC,PCC}$ (p.u.)) and AC voltage measured at the PCC in d coordinate ($V_{d,PCC}$ (p.u.)), (b) AC voltage measured at the PCC in q coordinate ($V_{q,PCC}$ (p.u.)), (c) Current reference for d coordinate ($I_{d,ref}$) and current measured at the PCC in d coordinate ($I_{d,PCC}$) and (d) Current reference for q coordinate ($I_{q,ref}$) and current measured at the PCC in q coordinate ($I_{q,PCC}$). 144
104 Verification of the solution based on the change in k_p to 1.65 in a weak AC grid for -20% variation of X/R: (a) Module of AC voltage measured at the PCC ($V_{AC,PCC}$ (p.u.)) and AC voltage measured at the PCC in d coordinate ($V_{d,PCC}$ (p.u.)), (b) AC voltage measured at the PCC in q coordinate ($V_{q,PCC}$ (p.u.)), (c) Current reference for d cooordinate ($I_{d,ref}$) and current measured at the PCC in d coordinate ($I_{d,PCC}$) and (d) Current reference for q cooordinate ($I_{q,ref}$) and current measured at the PCC in q coordinate ($I_{q,PCC}$). 146
105 Verification of the solution based on the change in k_i to 25000 in a weak AC grid for -20% variation of X/R: (a) Module of AC voltage measured at the PCC ($V_{AC,PCC}$ (p.u.)) and AC voltage measured at the PCC in d coordinate ($V_{d,PCC}$ (p.u.)), (b) AC voltage measured at the PCC in q coordinate ($V_{q,PCC}$ (p.u.)), (c) Current reference for d coordinate ($I_{d,ref}$) and current measured at the PCC in d coordinate ($I_{d,PCC}$) and (d) Current reference for q coordinate ($I_{q,ref}$) and current measured at the PCC in q coordinate ($I_{q,PCC}$). 147
106 A scalar function of two variables with three types of stationary points: minimum, maximum and saddle point [117]. 161
107 Illustration of Lyapunov's theorems on stability: (a) asymptotic stability and (b) instability [117]. 162
108 Equivalent impedance model [26]. 166
109 Nyquist paths according to stability (a) Stable Nyquist path, with no encirclements of -1+j0 and (b) Unstable Nyquist path, with an encirclement of -1+j0 [120]. 168

List of Tables

1 Short-circuit design values of the AC grid, PCC and VSC for the analysis required. . . . 121
2 AC grid parameters for different SCR values. . . . 121
3 AC line parameters for different levels of X/R deviation. . . . 122
4 Closed-loop system eigenvalues in a previous unstable case, i.e. SCR=2.34 and X/R=6.61, corresponding to the final red position in Figure 92(a). . . . 129
5 General configuration of each model in DIgSILENT PF . . . 170
6 EMT model parameters of AC line model in DIgSILENT PF . . . 171
7 EMT model parameters of the onshore VSC model in DIgSILENT PF . . . 171
8 EMT parameters of DC line of the bipolar HVDC configuration in DIgSILENT PF . . . 172
9 Control parameters of onshore VSC model in DIgSILENT PF . . . 172
10 EMT model parameters of the AC line of the wind park in DIgSILENT PF . . . 173
11 EMT model parameters of the offshore VSC model in DIgSILENT PF . . . 173
12 Model parameters of offshore transformer in DIgSILENT PF . . . 174
13 Control parameters of offshore VSC in DIgSILENT PF . . . 174
14 Model parameters of offshore wind park in DIgSILENT PF . . . 175
15 Parameters of the small signal model . . . 177

Nomenclature

Δu	Perturbation in u
ΔV_{DC}	DC voltage variation due to FSM function [p.u.]
Δx	Differential length of a Π equivalent section of the AC line [p.u.]
Δx	Perturbation in x
Δy	Perturbation in y
δ_{ij}	Phase angle difference between the V_i and V_j in a multi-infeed system [º]
λ	Eigenvalue
$\|V_{AC}\|$	Module of AC voltage [p.u.]
ν	Phase velocity [m/s]
Ω	Domain in Lyapunov theory
ω	Angular frequency parameter of PR controller[rad/s]
ω_0	Fundamental resonant angular frequency [rad/s]
ω_Δ	Energy difference of the MMC [J]
$\omega_{\Sigma,z}$	Zero-sequence component of energy sum of the MMC [J]
ω_Σ	Energy sum of the MMC [J]
ω_c	Cut-off angular frequency of non-ideal PR controller [rad/s]
ω_{grid}	Grid angular frequency [rad/s]
ω_{ij}	Phase angle difference between the i_{th} and j_{th} single-infeed HVDC systems in a multi-infeed system [º]
ω_i	Imaginary part of complex eigenvalue
Φ	Right eigenvector

ψ	Left eigenvector
σ_i	Real part of complex eigenvalue
θ	Grid angle
ζ_i	Damping ratio of complex eigenvalue
A	State matrix
B	Control matrix
$B_{c,i}$	Susceptance of shunt capacitors in a multi-infeed HVDC system[S]
C	Capacitance per length unit of the AC line [$\mu F/km$]
C	Output matrix
C_{eq}	Equivalent capacitor of the MMC [μF]
D	Feed-forward matrix
e_v^*	Contribution of grid current control of the MMC [p.u.]
f	Frequency [Hz]
f	State-space vector n non-linear functions
$f_{d,i}$	Damped frequency of complex eigenvalue
f_h	Frequency threshold for FSM function [p.u.]
f_{max}	Required frequency response for a specific accuracy in the representation of AC line model by several Π sections [Hz]
$f_{n,i}$	Natural frequency of complex eigenvalue
FSM_{th}	Frequency sensitive Mode (FSM) y-intercept
g	State-space vector m non-linear functions
h	Harmonic number
$H(x)$	Hessian matrix in Lyapunov theory
I	Identity matrix
$i_{2,d}$	AC current through the AC line in d coordinate [p.u.]

$i_{2,q}$	AC current through the AC line in q coordinate [p.u.]
$i_{3,d}$	AC current through the AC equivalent grid in d coordinate [p.u.]
$i_{3,q}$	AC current through the AC equivalent grid in q coordinate [p.u.]
$i_{c,d}$	AC current through the parallel capacitance of AC line in d coordinate [p.u.]
$i_{c,q}$	AC current through the parallel capacitance of AC line in q coordinate [p.u.]
$i_{c,z}$	Zero-sequence component of circulating current of the MMC [A]
i_c	Circulating current of the MMC [A]
$I_{d,PCC}$	AC current measured at the PCC in d coordinate [p.u.]
$I_{d,ref}$	Setpoint for d component of current in dq frame [p.u.]
i_d, i_q	Grid currents in dq frame of the MMC [p.u.]
i_g	Grid current of the MMC [A]
I_l	Load current source in impedance analysis
i_l	Lower arm current of the MMC [A]
I_{PCC}	Current at PCC in impedance analysis
$I_{q,PCC}$	AC current measured at the PCC in q coordinate [p.u.]
$I_{q,ref}$	Setpoint for q component of current in dq frame [p.u.]
$i_{s,Z}$	Circulating current [p.u.]
$i_{v,d}$	d component of grid current of the MMC [A]
$i_{v,q}$	q component of grid current of the MMC [A]
k_0	Constant related to sinusoidal modulation of VSC
$k_{droop,AC}$	Droop AC constant that relates reactive power with AC voltage in outer controller
k_{FSM}	Frequency Sensitive Mode (FSM) slope for frequency control in outer controller

k_i k_{i1}	Integral control constants for PR controller
k_p,k_{p1}	Proportional control constants for PR controller
k_q	Proportional constant in q component of proportional integral outer controller
k_v	Proportional constant in d component of proportional integral outer controller
L	Inductance per length unit of the AC line [mH/km]
L	Matrix of left eigenvectors
L_a	Arm inductance of the MMC [H]
L_f	Inductance of VSC output filter
l_u	Upper arm current of the MMC [A]
N_{eq}	Number of equivalent Π sections necessary to obtain the desired f_{max}
n_l	Insertion index in the lower arm of the MMC [p.u.]
n_u	Insertion index in the upper arm of the MMC [p.u.]
P_{aux}	DC power measured by the time a frequency deviation exceeds a threshold that activates an ancillary frequency function [p.u.]
$P_{DC,i,eq}$	Equivalent nominal active power of an HVDC system composed by several HVDC stations [MW]
$P_{DC,j}$	Active power injected by the j_{th} HVDC system in a multi-infeed system [MW]
$P_{DC,ref}$	Setpoint for DC power [p.u.]
P_{DC}	DC power [p.u.]
P_{DC}	Nominal active power of a single-infeed HVDC system [MW]
P_t	Infeed- wind power [p.u.]
Pmd	Modulation index in d coordinate [p.u.]
Pmd_{ss}	Modulation index in d coordinate in steady-state regime[p.u.]

Pmq	Modulation index in q coordinate [p.u.]
Pmq_{ss}	Modulation index in q coordinate in steady-state regime[p.u.]
$Q_{AC,ref}$	Setpoint for reactive power [p.u.]
Q_{AC}	Reactive power [p.u.]
Q_c	Reactive power of shunt capacitors [MVAr]
$Q_{DC,j}$	Reactive power injected by the j_{th} HVDC system in a multi-infeed system [MVAr]
Q_{droop}	Discontinuous function for calculating reactive power variations based on AC voltage variations
Q_{sa-max}	Maximum absorption limit of DFIG for reactive power [p.u.]
$Q_t(p.u.)$	Reactive power required to retain the rated voltage at POC. Negative and positive values correspond to absorbed and injected power, respectively [p.u.]
R	Matrix of right eigenvectors
R	Resistance (Ω)
R	Resistance per length unit of the AC line [Ω/km]
R_a	Arm resistance of the MMC [Ω]
R_f	Resistance of VSC output filter
$S_{AC,grid}$	Short-circuit power of the AC equivalent grid [MVA]
S_{cc}	Short-circuit power (MVA)
$s_{critical,0}$	Initial position of the trajectory of critical eigenvalue in the complex plane
$s_{critical,F}$	Final position of the trajectory of critical eigenvalue in the complex plane
S_N	Nominal power (MVA)
S_{PCC}	Short-circuit power measured at the PCC [MVA]

S_{VSC}	Short-circuit power of VSC [MVA]
SCR	Short-Circuit Ratio
SCR_{PCC}	Short-Circuit Ratio at the PCC
T_q	Time constant in q component of proportional integral outer controller
T_v	Time constant in d component of proportional integral outer controller
u	Column vector for state-space input
u_0	Column vector for state-space input at initial time
u_c^*	Contribution of circulating current control of the MMC [p.u.]
$V(x)$	Scalar function in Lyapunov theory
$V_{1,d}$	Voltage at the receiving end of the AC line in d coordinate [p.u.]
$V_{1,q}$	Voltage at the receiving end of the AC line in q coordinate [p.u.]
$V_{2,d}$	Voltage at the remote end of the AC line in d coordinate [p.u.]
$V_{2,q}$	Voltage at the remote end of the AC line in q coordinate [p.u.]
$V_{\alpha,PCC}$	AC voltage measured at the PCC in α coordinate [p.u.]
$V_{\beta,PCC}$	AC voltage measured at the PCC in β coordinate [p.u.]
$V_{AC,PCC}$	Module of AC voltage at the PCC [p.u.]
$V_{AC,ref}$	Setpoint for AC voltage [p.u.]
V_{AC}	AC voltage [p.u.]
v_{AC}	AC voltage of the MMC at the PCC [kV]
$v_{c,z}$	Zero-sequence component of common mode voltage of the MMC [kV]
$v_{Cl,i}$	Lower arm capacitor voltage of the MMC [kV]
$v_{Cu,i}$	Upper arm capacitor voltage of the MMC [kV]
v_c	Common mode voltage of the MMC [kV]

$V_{d,AC}$	AC voltage in d coordinate at the VSC output before the output filter [p.u.]
$V_{d,PCC}$	AC voltage measured at the PCC in d coordinate [p.u.]
$V_{d,ref,ss}$	Output voltage of PR controller in d coordinate in steady-state regime
$V_{d,ref}$	Output voltage of PR controller in d coordinate
$V_{DC,diff,ss}$	Mean value of the positive and negative DC voltage measurements in steady-state regime
$V_{DC,diff}$	Mean value of the positive and negative DC voltage measurements
$V_{DC,nom}$	Nominal DC voltage of the MMC [kV]
$V_{DC,ref}$	Setpoint for DC voltage [p.u.]
$V_{DC,ss}$	DC voltage in steady-state regime [p.u.]
V_{DC}	DC voltage [p.u.]
V_{DC}^{+},V_{DC}^{-}	Positive and Negative DC voltages measured at each pole of the HVDC link
V_j	Voltage at the j_{th} bus in a multi-infeed system [V]
v_l^{σ}	Measured upper arm voltages of the MMC [p.u.]
V_{PCC}	Voltage at PCC in impedance analysis
$V_{poc}(p.u.)$	Voltage measured at POC [p.u.]
$V_{q,AC}$	AC voltage in q coordinate at the VSC output before the output filter [p.u.]
$V_{q,PCC}$	AC voltage measured at the PCC in q coordinate [p.u.]
$V_{q,ref,ss}$	Output voltage of PR controller in q coordinate in steady-state regime
$V_{q,ref}$	Output voltage of PR controller in q coordinate
V_s	Source voltage in impedance analysis

v_s	Internal voltage of the MMC [kV]
v_u^σ	Measured upper arm voltages of the MMC [p.u.]
W	Stored energy in the MMC [J]
X	Reactance (Ω)
x	Column vector for state-space variable
X/R	Inductive-resistive characteristic
x_0	Column vector for state-space variable at initial time
X_{cc}	Short-circuit reactance [Ω]
x_{d1}, x_{d2}, x_{d3}	PR state variables in d coordinate
x_{q1}, x_{q2}, x_{q3}	PR state variables in q coordinate
x_q	Outer controller state variable in q coordinate
x_v	Outer controller state variable in d coordinate
y	Column vector for state-space output
Z	Impedance(Ω)
Z_l	Input impedance in impedance analysis
Z_s	Output impedance in impedance analysis
Z_z	Equivalent AC grid impedance in a single-infeed HVDC system [Ω]

Glossary

CCC Capacitor commutated converter

CM Compensated modulation

CSC Current source converter

CSC-PWM Pulse-width modulation current source converter

DAE Differential algebraic equation

DFIG Doubly fed induction generator

EMT Electromagnetic transient

ENSTOE European Network of Transmission System Operators

ESCR Effective short-circuit ratio

FACTs Flexible alternating current transmission systems

FRT Fault ride through

FSM Frequency sensitive mode

HVAC High-voltage AC current

HVDC High-voltage direct current

HVDC-VSC Voltage source converter in an HVDC application

LCC Line commutated converter

LFSM Limited Frequency Sensitive Mode

LMI Linear matrix inequalities

LVRT Low-voltage ride through

L-F Local frequency control strategy

MIESCR Multiple-infeed effective short-circuit ratio

MIMO Multiple input-multiple output

MMC Modular multilevel converter

MTDC Multi-terminal DC network

PCC Point of common coupling

PF Power factor

PI Proportional integral

PLL Phase-locked loop

PMU Phasor measurement unit

POC Point of connection

PQ Active power-reactive power

PR Proportional resonant

PRXC Proportional resonant controller with C feedback branch

PRXF Proportional resonant controller with X feedback branch

PRX2 Proportional resonant controller with X feedback and C branches

PVac Active power-AC voltage

PWM Pulse-width modulation

P2P Point-to-point

RES Renewable energy sources

RMS Root mean square

SCR Short-circuit ratio

SISO Single input-single output

uCM Uncompensated modulation

UPF Unity power factor

VdcQ DC voltage-reactive power

VdcVac DC voltage-AC voltage

VP Voltage-power

VSC Voltage source converter

VSC-AC VSC connected to an AC system

WAMS Wide area measurement system

WA-F Weighted average frequency control

X/R Inductive-resistive characteristic

2L-VSC Two-level voltage source converter

1 Introduction

The aim of this chapter is to provide the context and motivation of the PhD thesis, as well as the research questions it poses. Based on this, the scope and the contributions of the thesis are clarified, and the publications derived are listed. This chapter also presents the outline of the PhD thesis, chapter by chapter.

1.1 Context and motivation

1.1.1 HVDC-HVAC systems

There is an increasing interest worldwide in the development of a meshed high-voltage direct current (HVDC) transmission grid that connects load centres with huge renewable energy generation plants located at remote places.

Nowadays, the most commonly used topology for HVDC technology is the point-to-point (P2P) HVDC configuration, which is especially indicated for the evacuation of remote renewable energy into the AC grid, being suitable to convey energy from different energy sources [1].

At worldwide level, there has been more than 60 years of experience in HVDC projects, as shown in Figure 1. The future tendency is the interconnection of P2P HVDC links to create a mesh, which is known as multi-terminal DC (MTDC) topology. There are different organisations that want to develop these grids. Friends of the Supergrid [2] are advocating for a widely meshed MTDC grid but they recognise it may probably emerge more gradually as a combination of HVDC lines planned and built as independent projects. Advantages offered by an MTDC topology include enhanced reliability of the DC system, flexibility of power dispatch control, reduction of the intermittency of renewable energy and efficient utilization of power converters and cables.

In Figure 1 several of the existing MTDC projects are pinpointed, being New England and Sardinia-Corsica-Italy interconnections the most relevant due to their size and characteristics.

New England system is composed by three terminals operating at ±450kV DC, and it was developed in two commissioning phases, namely in 1986 and later in 1990-1992. The grid connects Quebec's extensive renewable energy resources to major population centres in southern New England at 315 kV (Radisson), 230 kV (Nicolet) and 345 kV (Sandy Pond) substations [3]. Nowadays, it is the only MTDC bipolar HVDC system in the world where the three stations operate under a common master control system.

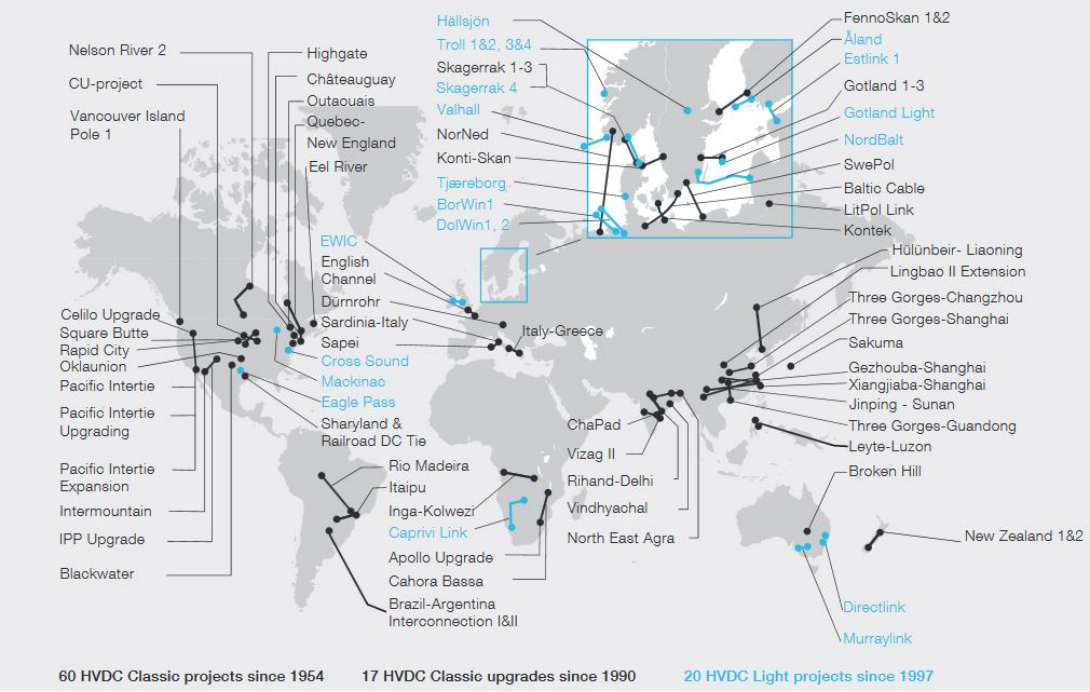

Figure 1: HVDC projects at worldwide scale [1].

Sardinia-Corsica-Italy was commissioned at the first stage in 1967 as a P2P mono-link operating at ±200kV DC and in 1988 and 1992 two more stations were added, configuring it into an MTDC topology [4]. The new connection with Sardinia allows to improve the stability for Sardinia's weak AC system. They are based on line commutated converters (LCCs), which provide technological maturity at the expense of limited reactive power control, inability of reversing current direction and the need of very complex master terminal control [5].

These projects have a limited number of terminals because it is necessary to reverse the voltage to change the direction of the power flow. To overcome these issues, the future MTDC grids will use voltage source converters (VSCs) as the key converter technology to interconnect AC and DC grids. This is due to the fact that VSC technology presents technical advantages over LCC, such as the ability to control active and reactive power independently, the provision of high controllability of DC grid, the change of the current flow direction and the black start capability [6].

HVDC-VSC has become the most feasible solution to the integration of remotely located large renewable energy plants, mainly due to its small footprint and its ability to support very weak AC systems. It also serves to connect AC systems operating at different frequencies.

There are forthcoming projects such as the North-East Agra, which is under construction in India with ±800 kV and 6000 MW and will occupy a total length of 1728 km [5]. This project will have three initial LCC stations at Biswanath, Chariali, Alipurduar and Agra, and will bring the installed capacity in two stages [5]. Besides, the Atlantic Wind Connection Project has been proposed by the United States and will be a subsea offshore backbone electrical transmission system of 7000 MW for offshore wind to be integrated in the corridor between Virgina and New York area [5]. The converters in this project will be rated 1000 MW at ±320 kV and will be configured as a symmetrical monopole [5]. There is also the Zhang-Bei project, which is a DC grid project aimed at securing power supply to the city of Beijing from a diverse set of renewable energy sources (RES), including wind, solar and hydro power. The Zhang-Bei project will be commissioned in its final version in 2021 and consists of four converter stations in the first stage with a half-bridge modular multilevel converter scheme with DC breaker, where one terminal of 3000 MW and ±500 kV receives power from three sending terminals of 1500 MW and ±500 kV each [5].

Regarding the topology of VSCs, two-level VSC has been widely employed. Its main feature is their capability of producing two output voltage levels, taking advantage of a simple circuitry and of the small size of DC capacitors. However, they need high blocking voltage capabilities in their rating and the output AC waveform contains high level of unwanted harmonics. As the power ratings have been increasing along the years, a greater number of levels must be added, with the emerging complexity regarding switching frequencies and delays in the output signal. Therefore, a new concept of VSC was designed, i.e. the modular multilevel converter (MMC) [7]. This can be basically described as an n level diode clamped converter which consists of n-1 capacitors on the dc bus and generates n levels of phase voltage and 2n-1 levels of output line voltage. Besides, the output waveform presents a better harmonic content compared to the two-level configuration. However, it presents other challenges to overcome, such as, the need of extra controller to balance the capacitor voltages, the circulating current, which has a double fundamental frequency component that increases the losses if not suppressed, and the need of monitoring each capacitor voltage [8].

Apart from two-level VSCs and MMCs, there are other configurations of VSC technology that are out of the scope of the present PhD thesis, such as the flying capacitor converter or cascaded-multilevel inverter. This is a developing technology with different proposals by several manufacturers: MMC offered by Siemens, MMC-FB proposed by G-S Alstom and Cmd by ABB.

It is interesting to analyse the behaviour of different VSC topologies in combination with specific AC grid configurations. The possibility of connecting VSCs with AC grids of different stiffness has been widely studied, but not when a variable X/R characteristic is considered.

1.1.2 Stability of HVDC-AC systems [9]

The concept of power system stability has been studied in detail by grouping different kinds of phenomena according to the magnitude affected, its severity and duration. In Figure 2, the concept of power system stability is presented as consisting into three main branches: voltage, frequency and rotor angle stability. These types of stability are hereafter defined according to [9].

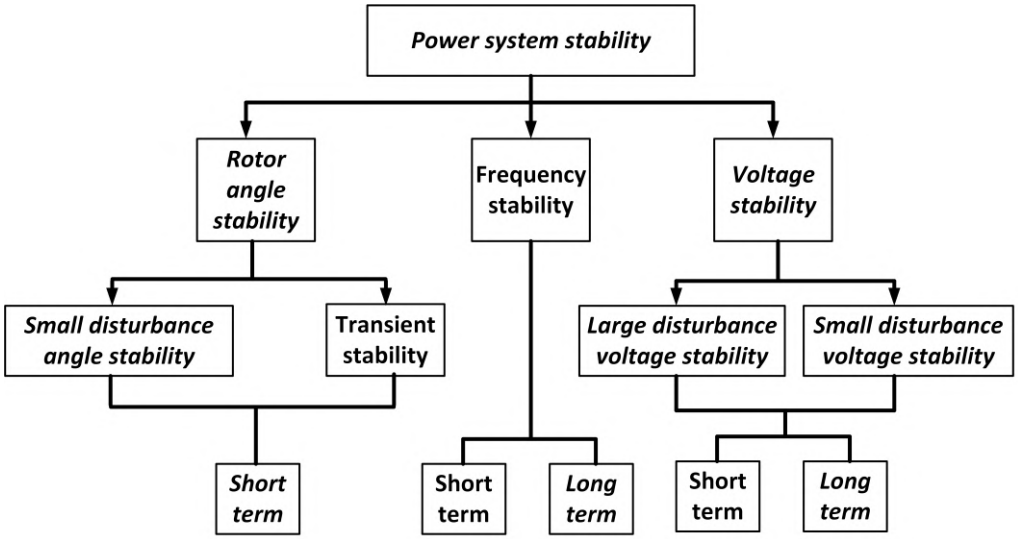

Figure 2: Definition of transient stability [9].

Rotor angle stability only considers short-term variations and is defined as the ability of synchronous machines of an interconnected power system to remain in synchronism after being subjected to a disturbance, where small disturbance (or small signal) rotor angle stability would cover small disturbances, such as poorly damped rotor oscillations, and transient stability would cover severe disturbances, such as short-circuits on a transmission line.

In the case of HVDC systems connected to AC grids, transient stability can be tested by applying a voltage dip at the point of common coupling. Voltage dips are short duration reductions in root mean square (RMS) voltage caused by diverse phenomena, such as, short-circuits or overloads [10]. Voltage dips constitute today a stability risk in networks with high penetration of renewable energy

[11], since they may cause the simultaneous disconnection of many renewable generators. As a consequence, the characteristics of the voltage time response that wind farms and other RES must be able to ride-through have been defined by many power system operators. This definition includes depth, duration and profile, as well as the exchange of active and reactive power that must be achieved during the disturbance.

Voltage and frequency stability are strongly related to the ability to maintain/restore equilibrium between load demand and load supply from the power system. Voltage stability is defined as the ability of a power system to maintain steady-state voltages at all buses in the system after being subjected to a disturbance from a given initial operating condition. Voltage collapse may appear if the sequence of events accompanying voltage instability leads to a blackout or abnormally low voltages in a significant part of the power system. Short-term voltage instability, being in the order of seconds, involves dynamics of fast acting load components such as induction motors or HVDC converters, while long-term instability may last minutes and considers lower acting equipment such as tap-changing transformers or generator current limiters, among others. The stiffness and the X/R characteristic of the AC grid also have a significant effect on the voltage stability.

Finally, frequency stability is referred as the ability of a power system to maintain steady frequency, following a severe system disturbance resulting in a significant imbalance between generation and load. Frequency instability may occur in the form of sustained frequency swings provoking the tripping of generating units and/or loads. Frequency is the key variable that relates the balance between generation and demand and thus determines the stability in AC grids. Therefore, whenever there is a frequency deviation the stability of the system is risked, and it is reflected as an imbalance in the active power equilibrium. Frequency stability can be maintained by means of partial load-shedding or generator connection (multiple load connection or generator disconnection), leading to over-frequency (under-frequency) events.

A model to estimate frequency deviation after a power mismatch event is needed for the re-parameterisation of frequency relays in load shedding schemes, estimating the amount of load re-connection, spinning reserve or wind power generation [12]. According to the models to estimate frequency and voltage deviations, network operators design the grid codes in order to ensure stability on the entire electrical power system. A grid code describes the minimum technical and organizational requirements that must be fulfiled when setting up and operating

grid connections on the high voltage or extra high voltage grid [13]. Additional requirements may also be necessary for operation. These minimum requirements are set to ensure a stable and secure operation of the whole electrical system within a country or set of countries, and the grid codes are mainly designed for the operation of conventional technology, i.e. AC systems. Since one of the main applications of MTDC networks, and by extension the HVDC technology, is to convey huge amounts of renewable energy from remote areas, grid codes are expected to be updated with pertinent changes that take into account the variable nature of transmitted renewable energy, and also due to the new HVDC-AC interconnection facilities. However, the presence of HVDC grids may increase the DC component as a form of power quality distortion in AC grids, especially when AC and DC transmission lines are in proximity [14].

Besides, there is a tendency to harmonise grid codes in order to facilitate energy exchanges within and among countries, so that this harmonization will enable an improved operation considering the increase of complexity due to the inclusion of HVDC technology. Nevertheless, the increase of complexity will also jeopardise the stability of the system and therefore this deserves huge research efforts to avoid adverse interactions between HVDC technology and conventional AC systems.

It is the task of the control architecture of HVDC systems not only to meet technical requirements, as indicated by local grid codes, but also to guarantee the evacuation of energy in safe, efficient and secure conditions. In contrast to AC grids, where frequency remains constant over all stationary system, in HVDC grids DC voltage is different at each terminal due to the voltage drop in DC lines. So, each terminal will receive different voltage setpoints and this poses a challenge whenever the stability of an HVDC-AC system is considered.

These differences in stability principles between AC and HVDC grids, changes the way stability is traditionally studied and therefore, deeper research efforts must be done to accommodate both control paradigms and power theories, so no adverse interactions that risk the stability occur.

1.2 Problem statement and research questions

1.2.1 Current controllers in VSCs connected to AC systems

VSCs play an important role on the stability of both HVDC and AC networks. Being VSC the key HVDC technology, its inner current controller assumes a huge responsibility on the stability of the VSC [15]. Most of the inner controllers are

based on proportional integral (PI) controllers [16–21], but other less common control structures, such as proportional resonant (PR) controllers [22–24], can be found in the literature. As said, many current controllers have been implemented by means of PI blocks, but stability analysis becomes more complex when PR blocks are used for the inner current controller of a VSC. This is because the transfer function of PR blocks depends on the target angular frequency. However, PR blocks are chosen over PI due to the additional functionality they offer, such unbalanced faults handling or harmonics filtering.

In the last decade, PR controllers have appeared as an alternative to PI controllers, due to their unique behaviour under unbalanced operation [22] and the elimination of steady-state errors [22–25]. PR controllers operate in stationary frame, which allows them to track both balanced and unbalanced current references and provide an improved response under unbalanced faults in comparison to the response provided by PI controllers. Besides, with PR controllers the grid current waveforms are enhanced when interface inductors are not perfectly balanced between the phases.

Apart from these, other benefits of stationary-frame controllers are identified in [25]. One of them is the removal of the phase-locked loop (PLL), which eliminates errors due to synchronisation problems. Another advantage is the elimination of inverse Park transformations, which reduces overall computational burden. However, PR controllers have time-invariant modulation blocks in their control loop, which inhibits the use of parameterisation techniques such as eigenvalue analysis. Therefore, in order to study their impact on stability, a proper linearisation of the PR controller is needed, as proposed in [22]. The conversion can be carried out using a simple block diagram manipulation approach where the transfer function in stationary frame is converted to dq-frame, since the linearisation must be achieved around a sinusoidal linearisation point. Once linearised, the resulting equations can be arranged into parametric state-space format, so that the effects of controller gains, parameter values and operating point on the system stability can be explored. The effects of PR parameters on stability have been evaluated through the proportional constant and integral constant, which impact the time response and the damping of the system, respectively.

Different types of impacts have been assessed in the literature and this relates to the general classification of PR controllers detailed in section 2.6 of chapter 2, where the impact of each PR topology on stability is discussed.

Therefore, having discussed the main advantages of PR controller over PI controller, this PhD thesis is from now on focused on studying the effects of PR

controller parameters on stability for different AC grid characteristics.

1.2.2 Analytical methods to study the small signal interaction between VSCs and AC grids

The small signal stability of a power electric system can be studied according to different approaches found in the literature, as Figure 3 shows. In principle, two main different ways of analysing the small signal stability are taken under consideration, i.e. the model- and the measurement-based approaches.

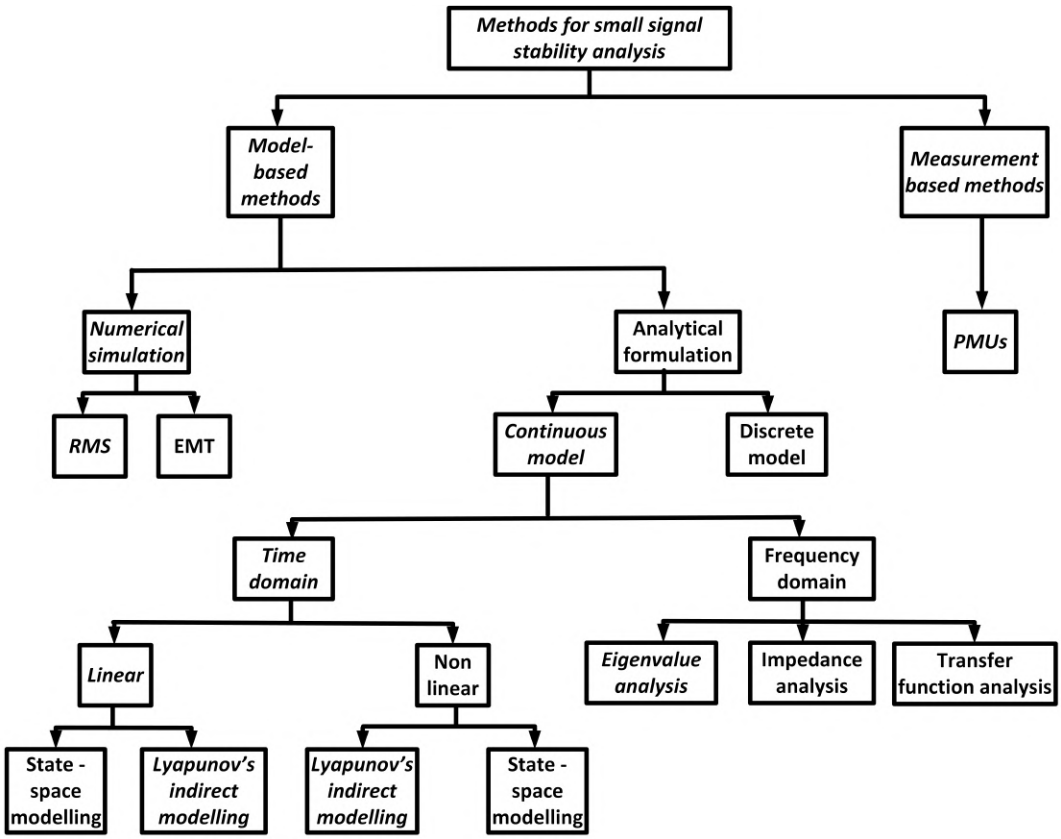

Figure 3: Classification of small signal stability [26, 27].

The measurement-based approach uses data measured by phasor measurement units (PMU). A PMU measures the frequency in voltages, currents and their phasors, by using synchronized measurements from the sampled data. PMUs are built to form a network named wide area measurement system (WAMS) [27]. In order to study the small signal stability problem, one of the most used methods is the linearised differential algebraic equation (DAE). DAE is a mathematical

model to develop eigenvalues and participation factors for the system that is being disturbed [27].

Regarding the model-based approach, two categories are found: numerical simulations and analytical formulations.

Numerical simulations have been widely used to prove the stability of a system under small disturbances in the frequency domain, using RMS simulations, and in the time domain, using EMT simulations. RMS simulations are valid for linear systems and take advantage of the simplicity, easiness and low computational burden, thus making simulations faster thanks to its linearised blocks [28]. However, inaccuracies appear whenever a non-linear system is tackled. For these cases, EMT simulations provide a detailed non-linear representation of a dynamic network model for electromagnetic and electro-mechanical transients under balanced and unbalanced network condition, treating non-linearities at the expense of higher computational burden [28].

The analytical formulation implies the derivation of algebraic expressions which represent the power system behaviour by means of either discrete or continuous domain. On the one hand, the discrete equations of a power system have been employed in literature, such as in [29], to obtain a more robust design of controllers at the cost of dealing with digital implementation and the selection of a proper discretisation technique. On the other hand, the continuous domain analysis is divided into time and frequency domain methods, though it is not able to obtain that robust designs. However, it takes advantage over the discrete analysis since it does not need a discretisation technique to sample the signal and simpler analytical approaches are obtained.

Within time domain methods, the state-space modelling method is widely used and consists in a representation of m_{th} order non-linear differential equations of a power system that relates its main state variables with inputs and outputs. The output, being a function of the state-variables, is used to see if the system is stable or not [27]. Another time domain analytical formulation is the Lyapunov method, which implies the definition of scalar functions that are used to prove the stability of an equilibrium operating point of a power system represented by its ordinary differential equations [30].

There is another version of both time domain analytical formulations, where non-linear operations, such as multiplications or coordinate changes, are linearised and therefore, further modifications on the previous equations are included. In the case of Lyapunov method, instead of looking for a scalar function to be

applied directly to the non-linear system, the system can linearised around the origin and attempt to discuss local stability of the origin, by using quadratic functions for the linearised system [30].

Regarding frequency domain methods, eigenvalue impedance and transfer function analysis are considered. Eigenvalue analysis studies power system's behaviour through calculating the eigenvalues of the system's model. In order to get the eigenvalues of a power system, a linearising process is necessary. The eigenvalues are the complex roots of the characteristic equation specific for the power system under consideration. Only when the eigenvalues are on the left side of the imaginary plane the system is stable.

As for the impedance-based analysis, it consists in calculating the AC or DC equivalent impedances of passive components, such as AC or DC line impedances, and in modelling with Norton or Thevenin equivalents the active components, such as VSCs, current and/or Voltage sources. By having computed the total impedance of the system under study, further analysis can be made by using Nyquist or Bode diagrams in order to determine the stability margin of a power system. The authors in [31] compare both eigenvalue and impedance-based methods and conclude that both can effectively determine the stability of the system, but at the expense of certain weaknesses. As stated in [31], the impedance-based analysis determines not global but local stability, making it necessary to investigate the impedance-based stability at all possible subsystems. However, it does not require such deep level of details, since the open-loop poles are sufficient for the analysis. On the contrary, the eigenvalue-based method, as said in [31], can determine the stability of the global system, but it cannot predict high level of details, such as the harmonic oscillations caused by a pulse-width modulation (PWM) converter operating in a stable point.

In [32], the transfer function-based stability analysis method is developed, where the poles and zeros of each subsystem, instead of the eigenvalues, are extracted by means of their transfer functions. It is mainly employed to tune the control-loop of the converters and does not include the effect of grid impedance.

It is interesting to discuss how one analytical time domain-based method, such as the state-space modelling analysis, could be validated by a numerical EMT simulations method, by taking into account discontinuities presented in the EMT model and how they are treated in the state-space system by applying a proper linearisation technique. It is also advisable to verify the conclusions by simulations with EMT models. These are essential pre- and post-analysis stages,

respectively, which have not been addressed in detail in the literature and therefore, deserve attention.

In appendix A, a deeper overview on the main analytical methods to study the small signal stability of the system is provided. These methods are classified according to time and frequency formulations. In the end a brief comparative discussion is made within each type of formulation.

1.2.3 Small signal interactions between VSC converters and AC grids

Important active power mismatches in AC grids can result into significant temporary frequency excursions, which might jeopardise power system stability [33]. In this respect, several generation assets, control and protection systems can contribute to mitigate the problem efficiently in a cooperative way. HVDC networks can also contribute to AC system frequency support, while ensuring the compliance of local grid codes [5].

The characteristics of an AC power system have also an influence on the stability of the VSC connected to an AC system (VSC-AC). An AC grid can be characterised by the short-circuit ratio (SCR) and the X/R ratio at the point of common coupling (PCC) of the VSC. SCR measures the AC grid strength while X/R ratio characterises the resistive-inductive behaviour. While the SCR ratio is dependent on the grid impedance, the X/R ratio indicates the angle of the current that flows through the AC grid. Thus, these two indicators are independent from each other and represent complementary aspects to analyse the tendency of an AC grid to lose stability.

Besides, the presence of many VSCs in the future MTDC grid will generate more control interactions, not only with other VSCs but with different AC grid characteristics and controls [34, 35]. And in the end, small perturbations, such AC transients in different current and voltage magnitudes, will provoke effects on the stability of several domains of the system [34, 35].

There have been projects of VSC interconnection whose instability has been widely studied in the case of weak AC grids [36]. However, they have not considered their integration into AC weak grids with a variable X/R characteristic.

Based on the last reasons, this PhD thesis is aimed at studying the interaction of an HVDC-VSC interconnection with AC grids of different SCR and X/R characteristics.

1.3 Scope of the thesis

The focus of the present PhD thesis is to design a methodology to tune the PR controller parameters of an AC grid-connected VSC, considering scenarios not very explored so far. These scenarios encompass combined changes in SCR and X/R ratios due to eventualities of diverse nature in the AC grid, such as sudden opening or closing of a circuit breaker at a specific speed, new connections to distribution or transmission grids or the modification of distance between conductors in electrical lines, under others. The methodological process sheds light on cases where the PR controller is well designed for a weak grid scenario, but loses stability with the change of the X/R ratio.

The thesis is aimed at the analytical research of the small signal interaction phenomena between controller parameters of VSC and AC grids and the verification of such analysis via EMT numerical simulations. The simulations determine the degree of accuracy of the corresponding scenarios. The results of this investigation detect combinations of PR parameterisations and AC grid topologies that lead to small signal instability issues, while at the same time identify implications for tuning PR controllers to avoid these adverse interaction phenomena. Different research gaps were identified at the beginning of the present PhD thesis:

- *Methodological tools to detect unexpected small signal instability issues, resulting from the interactions between a VSC and an AC grid.*
- *The exploration of scenarios defined by variability of the X/R ratio in weak AC grids* that lead to small signal instability issues.
- *Implications for tuning PR controllers of VSCs when subjected to the mentioned scenarios.*
- *The analysis of how the accuracy of MMC model, with compensated modulation control scheme, affects the conclusions yielded in the previous analysis.*

In order to contribute to solve these research questions, eigenvalue trajectory analyses have been performed for the complete VSC-AC system, starting from the state-space equations. New explanations and guidelines for the proper configuration of scenarios to detect unstable cases are given and at the same time, tuning implications for PR parameters are deduced.

1.4 Main contributions of the thesis

The lack of research centred around PR current controllers governing VSCs, jointly with the need to assess how they impact on specific AC grid configurations with different SCR and X/R ratios, has been identified. This poses challenges related to the progressive weakening of AC networks with the advent of the massive integration of renewable energies.

Two mathematical tools have been used to model the core of the methodological process. On the one hand, the state-space representation has been used to construct a small signal model of the system under study. On the other hand, the eigenvalue trajectory analysis has been carried out to analyse the impact of PR controller parameters of the VSC on the small signal stability when the AC grid has a variable X/R ratio.

This work has contributed to the area of small signal stability analysis of PR current-controlled VSCs connected to AC grids. The contributions of the thesis are hereafter summarised:

- *Development of a methodological tool or guideline to identify unexpected small signal instability issues of a VSC connected to an AC grid.* The methodological approach proposed by this PhD thesis can help researchers when trying to identify sources of unexpected instabilities in a system.

- *Identification of weak AC grid scenarios that with the change of X/R characteristic compromise and lose the stability.* So far, small signal stability studies in weak AC grids have considered the reduction of SCR values but not combined with slight modifications in X/R ratio. These scenarios have been found through a deep review in the literature. Besides, the scenarios and conclusions of the present work may help grid code makers when defining local connection requirements of VSCs.

- *Development of a methodology which extracts implications for tuning PR current controlled VSCs connected to AC grids with variable strength and X/R ratio.* For this purpose, a small signal model of a PR controlled VSC connected to an AC grid has been constructed and numerically validated. A systematic procedure for eigenvalue trajectory analysis is proposed to address the variable X/R characteristic of the AC grid. Besides, the cases extracted from the methodology have been verified by EMT simulations, and the methodology has been justified to be extended to modular multilevel converters under the compensated modulation control approach.

1.5 List of publications

Accepted journal papers

[1] Marta Haro-Larrode, Maider Santos-Mugica, Pablo Eguia, Raul Rodriguez-Sanchez and Asier Gil-de Muro, Impact of proportional resonant controller parameters of VSC connected to AC grids with variable X/R characteristic on the small signal stability, International Journal of Electrical Power Energy Systems, Volume 118, 2020, 105746, ISSN 0142-0615, https://doi.org/10.1016/j.ijepes.2019.105746.

Journal papers under review

[2] Marta Haro-Larrode, Maider Santos-Mugica, Agurtzane Etxegarai and Pablo Eguia, Methodology for tuning MTDC Supervisor and Outer Loop Control Systems under over-frequency events, under review in Energies Journal, Section:Electrical Power and Energy System.

Accepted conference papers

[3] M. Haro-Larrode, M. Santos-Mugica, A. Etxegarai, P. Eguia, Integration of offshore wind energy into an island grid by means of a Multi-Terminal HVDC-VSC network, in: 2018 Thirteenth International Conference on Ecological Vehicles and Renewable Energies (EVER), Monte-Carlo (Monaco),10th to 12th April 2018: pp. 1–6. doi: 10.1109/ EVER.2018.8362339.

[4] M.Haro-Larrode, Í.V. Temez, S.C. Recio, M.S. Mugica, P.E. Lopez, Integral control of a Multi-Terminal HVDC-VSC transmission system, in: 2017 Twelfth International Conference on Ecological Vehicles and Renewable Energies (EVER), Monte-Carlo (Monaco), 11th to 13th April 2017, pp. 1–15. doi: 10.1109/EVER.2017.7935938.

Accepted conference posters

[5] Marta Haro Larrode, Pablo Eguia Lopez, Maider Santos Mugica and Raúl Rodriguez Sánchez, "Small signal modelling and analysis of an offshore HVDC transmission link", V Marine Energy Conference, Euskampus Fundazioa, 13-11-2018, Bilbao (Spain).

[6] Marta Haro Larrode, Pablo Eguia Lopez, Maider Santos Mugica, Agurtzane Etxegarai Madina and Susana Apiñaniz Apiñaniz, "Validation of the Control structure of a Multi-Terminal HVDC (MTDC) grid for marine energy integration under adverse onshore AC grid fault phenomena", IV Marine Energy Conference, Euskampus Fundazioa, 20-11-2017, Bilbao (Spain).

[7] Marta Haro Larrode, Pablo Eguia Lopez, Maider Santos Mugica, Agurtzane Etxegarai Madina and Susana Apiñaniz Apiñaniz, "Grid Integration of Marine Energy by Means of HVDC Technology", III Marine Energy Conference, Euskampus Fundazioa, 17-11-2016, Bilbao (Spain)

Other publications

[8] E. Robles, M. Haro-Larrode, M. Santos-Mugica, A. Etxegarai, E. Tedeschi, Comparative analysis of European grid codes relevant to offshore renewable energy installations, Renewable and Sustainable Energy Reviews. 102 (2019) 171–185. doi: 10.1016/j.rser.2018.1 2. 002.

[9] P. Eguia, G. Gil, R. Rodriguez-Sanchez, M. Haro-Larrode, A. Gil-de-Muro, Characterization of network harmonic impedance for grid connection studies of renewable plants, International Conference on Renewable Energies and Power Quality (ICREPQ'18), Salamanca (Spain), 21th to 23th March, 2018.

1.6 Outline of the thesis

The thesis is structured as follows:

- In chapter 2, the main topologies of power converters are briefly described and summarised. From this list VSC technology is chosen, so that the next sections are focused only on VSC. Afterwards, the importance of the stiffness and X/R characteristic is highlighted for an AC grid connected to a VSC. Based on this, the main connection requirements for a VSC to an AC grid are listed according to an specific grid code. The state of the art of control structures for VSCs is presented. For this purpose, the main control schemes for VSCs at different layers are described, ranging from the MTDC to outer and inner control layers. As for the inner control layers, PI are compared to PR controllers. Having discussed the advantages of PR over PI controllers, several types of PR controllers are described according to the literature. Additionally, a specific section including an overview of the main operating principles of the MMC is provided. In the last part, a state of the art on the small signal interactions between VSCs and AC grids is presented, with especial focus on the HVDC environment. Besides, the main gaps in the literature are extracted, according to the content of the previous sections.

- In chapter 3, the methodology proposed by this PhD thesis is presented by means of a flowchart and described step by step. The state-space equations

for each subsystem that is part of the whole interconnected VSC-AC domain are presented. Several modelling approaches as well as linearisations are discussed. Based on this, the full small signal model is constructed. Besides, hypotheses relevant to the compensated modulation approach are discussed and the extension of the studies for the MMC is justified.

- In chapter 4, the application case of this PhD thesis is presented. In the first part, the small signal model is validated against EMT simulations and several preliminary tests are also included. Several VSC control parameters are justified by using Bode diagrams and time responses. As a result, the small signal model is prepared for eigenvalue analysis. In the second part, the eigenvalue trajectory analysis is presented to study the impact of PR parameters, SCR and X/R ratios on the small signal stability. The analysis is divided in two stages: one considering a constant X/R characteristic and another considering a variable X/R characteristic. The study has been complemented with a participation factor analysis to clarify the relationship between the critical eigenvalues and the state variables of the system. Several implications on the tuning of PR controller parameters are extracted.

- In chapter 5, the cases extracted in chapter 4 are verified by means of EMT simulations carried out in DIgSILENT PF, and contextualised with occurring phenomena in the AC grid.

- In chapter 6, the main conclusions derived from the methodology are presented. Besides, several limitations of the methodology are discussed. The future lines which could continue this work are also described.

- In the appendices, several theoretical and practical aspects are included to complement the document. In appendix A, the main analytical methods for stability analysis are classified and described in terms of time and frequency formulations. Besides, a discussion of methods is developed in order to stand out the advantages and disadvantages of each one. In appendix B, the EMT model parameters to validate and verify numerically the small signal model are gathered in several tables. In appendix C, the parameters of the small signal model are detailed in a table.

5 Verification of the methodology

5.1 Introduction

This chapter is aimed at verifying the cases extracted from the eigenvalue trajectory analysis by means of EMT simulations conducted in DIgSILENT PF.

Besides, in order to consider features related to the protection system, a threshold voltage is considered for the module of voltage at the PCC, which must not be exceeded except for transient peaks whose duration is less than 100 ms.

5.2 Model used for the verification of the methodology

The methodology is verified by conducting EMT simulations in DIgSILENT PF of the system presented in section 4.1.1 of chapter 4. The whole model and control parameters of the mentioned model are gathered in appendix B.

5.3 Verification of cases with constant X/R characteristic

In Figure 97 a PR parameterisation corresponding to the stable area (k_i=30000 and k_p=1.5) in a stiff AC grid (SCR=25) with X/R set to 8.37 is verified under a perturbation of 1% in $V_{DC,ref}$, starting at t=1s and ending at t=1.5s.

As noted in Figure 97(a) and Figure 97(b), the transient behaviour of $V_{d,PCC}$ and $V_{q,PCC}$ due to the perturbation presents an oscillatory period less than the duration of the perturbation.

Besides, Figures 97(a), 97(b) present transient peaks that exceed the threshold voltage at only one instant. In the zoomed area presented in Figure 97(a) it can be seen that the $V_{d,PCC}$ signal matches accurately the $V_{AC,PCC}$ signal, as expected due to the stiff nature of the AC grid and to adequate PLL parameterisation.

As for $I_{d,PCC}$ and $I_{q,PCC}$ shown in Figure 97(c) and Figure 97(d), they follow their corresponding setpoints $I_{d,ref}$ and $I_{q,ref}$ at the input of the PR controller.

The signals presented along Figures 97(a), 97(b),97(c) and 97(d) demonstrate a stable case for the chosen PR parameterisation, under a perturbation of 1% of the $V_{DC,ref}$ value.

As for a weak AC grid case (SCR=2.3), the same PR parameterisation is chosen to be verified and the corresponding signals shown in Figure 98.

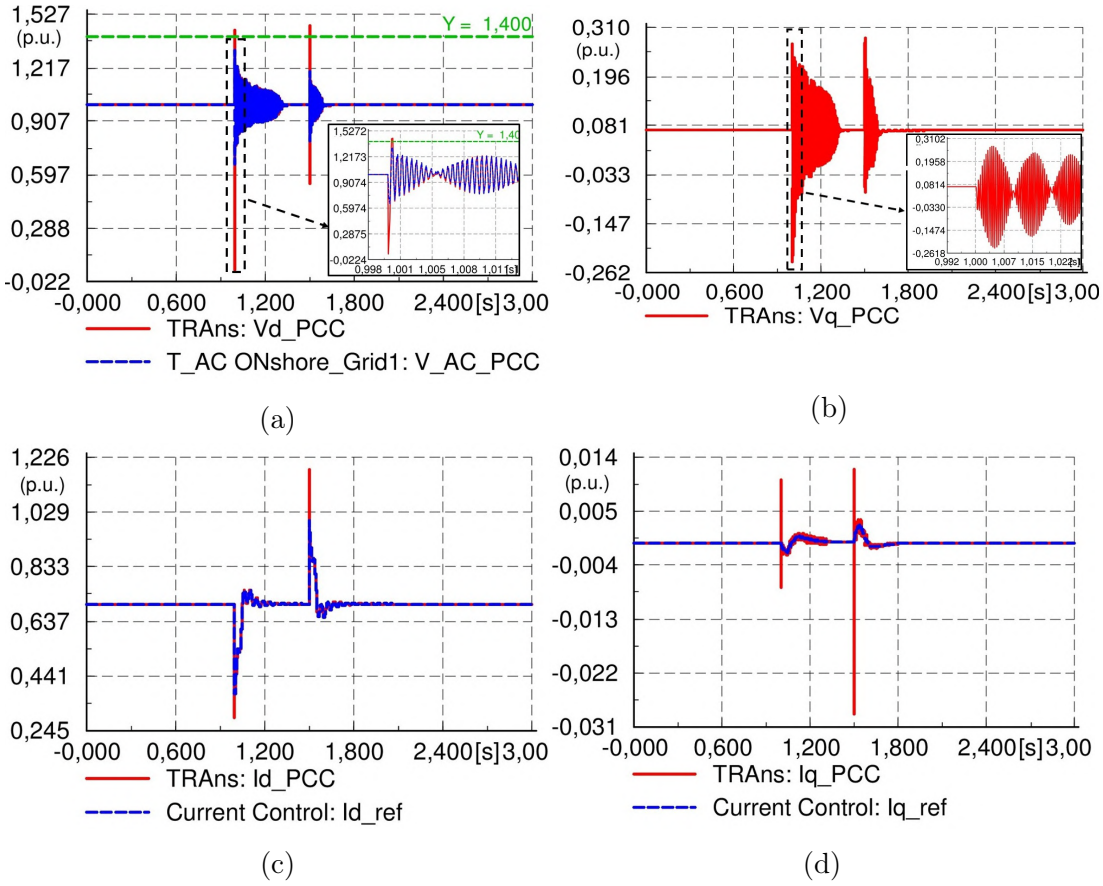

Figure 97: Verification of a stiff AC grid: (a) Module of AC voltage measured at the PCC ($V_{AC,PCC}$ (p.u.)) and AC voltage measured at the PCC in d coordinate ($V_{d,PCC}$ (p.u.)), (b) AC voltage measured at the PCC in q coordinate ($V_{q,PCC}$ (p.u.)), (c) Current reference for d coordinate ($I_{d,ref}$) and current measured at the PCC in d coordinate ($I_{d,PCC}$) and (d) Current reference for q coordinate ($I_{q,ref}$) and current measured at the PCC in q coordinate ($I_{q,PCC}$).

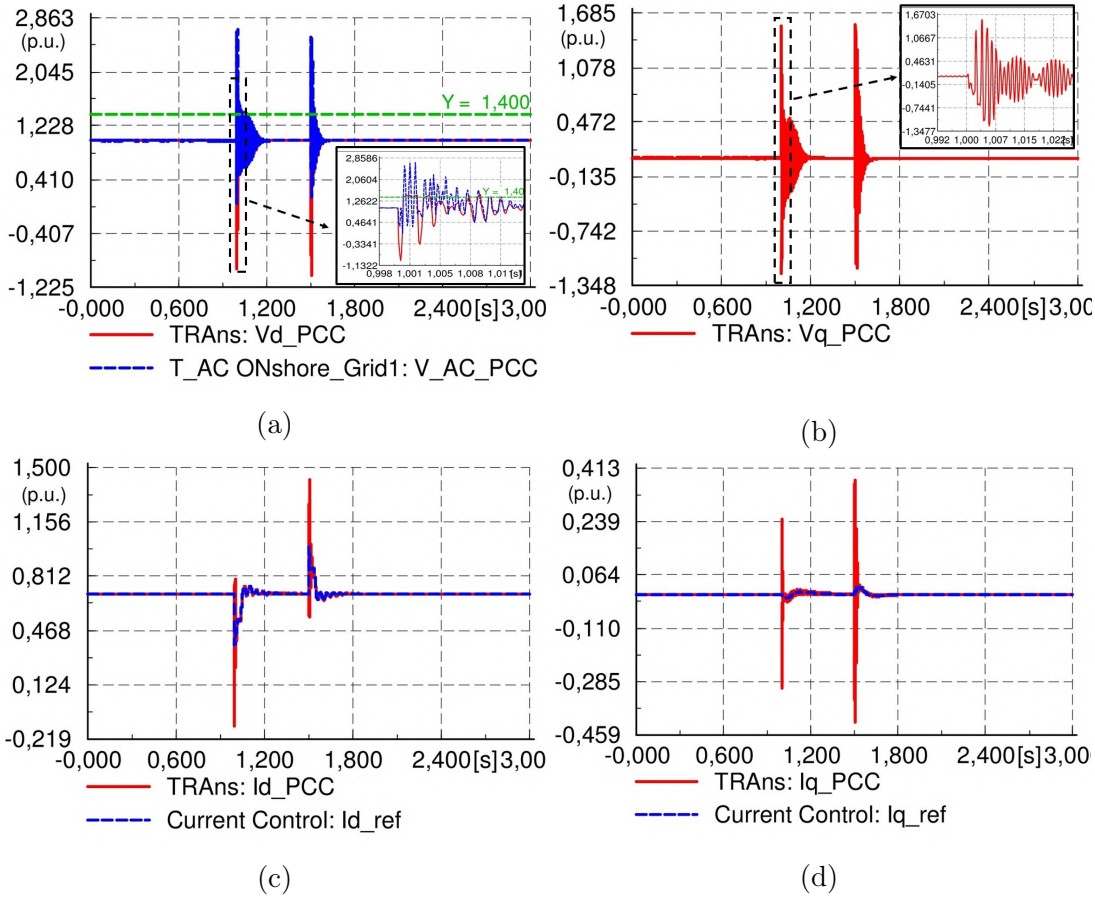

Figure 98: Verification of a stable case in a weak AC grid: (a) Module of AC voltage measured at the PCC ($V_{AC,PCC}$ (p.u.)) and AC voltage measured at the PCC in d coordinate ($V_{d,PCC}$ (p.u.)), (b) AC voltage measured at the PCC in q coordinate ($V_{q,PCC}$ (p.u.)), (c) Current reference for d coordinate ($I_{d,ref}$) and current measured at the PCC in d coordinate ($I_{d,PCC}$) and (d) Current reference for q coordinate ($I_{q,ref}$) and current measured at the PCC in q coordinate ($I_{q,PCC}$).

The case shown in Figure 98 corresponds to a stable case in a weak AC grid with SCR=2.3, with the same PR parameterisation as in Figure 97.

In contrast to the case presented in Figure 97(a), in Figure 98(a) the oscillations belonging to the transient period of $V_{AC,PCC}$ and $V_{d,PCC}$ have a larger amplitude than in 97(a), and thus the voltage threshold is exceeded at several instants during the beginning and the end of the perturbation, as expected due to the decrease in SCR. The zoomed area in Figure 98(a) shows that $V_{d,PCC}$ signal deviates transiently from $V_{AC,PCC}$ signal but finally converges to $V_{AC,PCC}$. This is expected due to the weak nature of the AC grid. According to this observed detail, the PLL parameterisation allows also a good accuracy.

Besides, since the peaks do not exceed the voltage threshold continuously, but they alternate with valleys and the overtaking lasts less than 100 ms, this phenomenon does not endanger the protection system of the VSC. As for the currents in Figure 98(c) and 98(d), $I_{d,PCC}$ and $I_{q,PCC}$ follow their respective setpoints $I_{d,ref}$ and $I_{q,ref}$ with peaks of increased value with respect to those observed in Figure 97(c) and 97(d).

Apart from this, the effect of decreasing k_p to lower values than 0.3 in a weak AC grid case is verified in Figure 99. In Figure 99(a) $V_{d,PCC}$ does not align to $V_{AC,PCC}$, as seen in the zoomed area, and both $V_{d,PCC}$ and V_{AC_PCC} exceed permanently the voltage threshold by the time the perturbation begins, driving the system into instability.

The same behaviour is observed in $V_{d,PCC}$, $I_{d,PCC}$ and $I_{q,PCC}$, with the increase of oscillation amplitude permanently from the beginning of the perturbation on.

Figure 97, Figure 98 and Figure 99 confirm the implications for tuning the PR controller of VSCs in AC grids with constant X/R characteristic, extracted in section 4.2.2 of chapter 4.

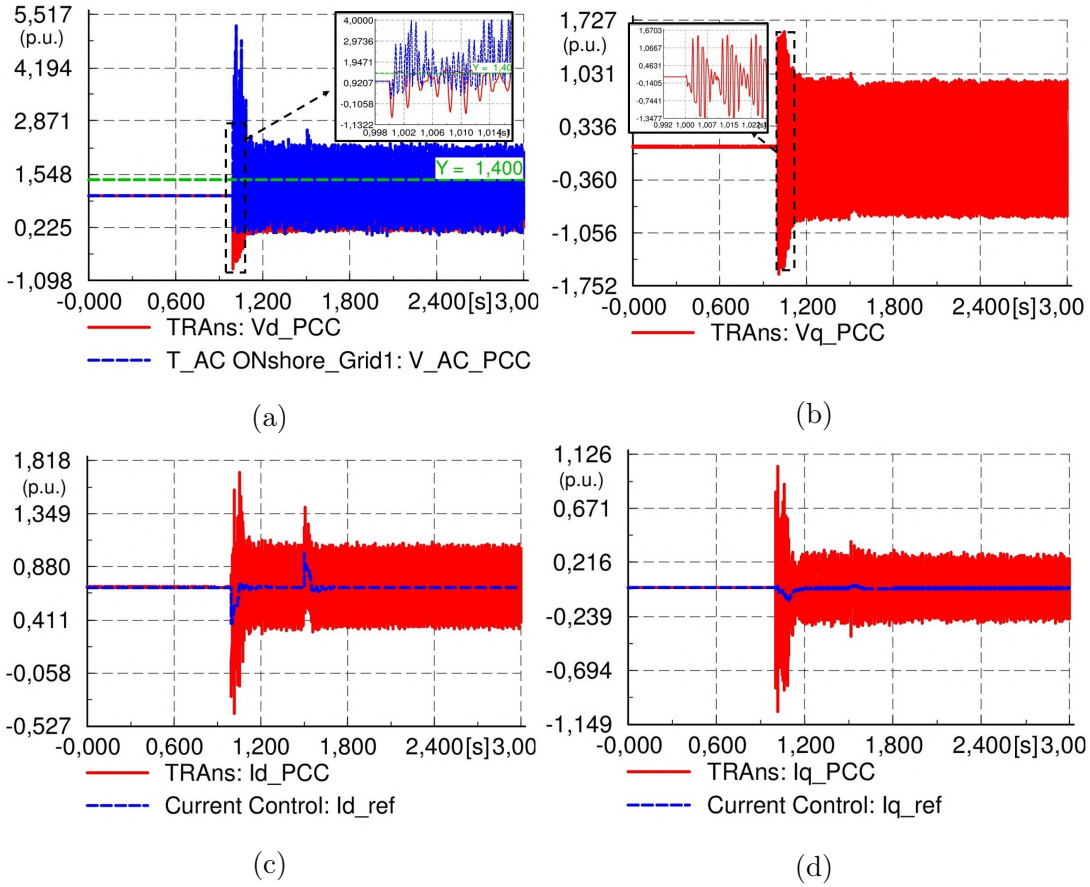

Figure 99: Verification of an unstable case in a weak AC grid for k_p=0.1 and k_p=30000: (a) Module of AC voltage measured at the PCC ($V_{AC,PCC}$ (p.u.)) and AC voltage measured at the PCC in d coordinate ($V_{d,PCC}$ (p.u.)), (b) AC voltage measured at the PCC in q coordinate ($V_{q,PCC}$ (p.u.)), (c) Current reference for d cooordinate ($I_{d,ref}$) and current measured at the PCC in d coordinate ($I_{d,PCC}$) and (d) Current reference for q cooordinate ($I_{q,ref}$) and current measured at the PCC in q coordinate ($I_{q,PCC}$).

5.4 Verification of cases with variable X/R characteristic

The base PR parameterisation, k_p=1.5 and k_i=30000, is now tested against a weak AC grid (SCR=2.3) with variable X/R characteristic, ranging from -20% to +20% of the usual value, 8.37.

In Figure 100, it is tested in a weak AC grid with X/R=6.61, where the X/R ratio has been lowered by a 20% from its usual value. The behaviour of $V_{d,PCC}$ and V_{AC_PCC} in Figure 100(a) shows the unstable behaviour of the system, being similar to the one observed in Figure 99(a). This also makes the currents $I_{d,ref}$ and $I_{q,ref}$ oscillate and not follow their setpoints once the perturbation is introduced, as shown in Figure 100(c) and in Figure 100(d).

In Figure 101, the system is tested in a weak AC grid with X/R=7.5, where the X/R ratio has been lowered by a 10% from its usual value. This presents similar results as in Figure 100.

As seen in Figure 100(a) and 101(a), the zoomed image of signals presents oscillations that exceed permanently the threshold value for longer time than 100ms. This also provokes the increase of amplitude in the currents from the beginning of the perturbation, as deduced from Figure 101(c) and Figure 101(d).

The stable cases derived from the positive variations of X/R ratio, namely the +10% and +20%, have been also verified in Figures 102 and 103, respectively. These cases were stable according to the analysis conducted in section 4.2.3 of chapter 4.

In both Figures 102(a) and 103(a), it can be observed that $V_{d,PCC}$ and $V_{AC,PCC}$ exceed the threshold for less time than 100 ms. The zoomed section of the signals shows the reduction of oscillation amplitude progressively until the signals converge to their steady-state values, in contrast to the behaviour observed in Figures 100(a) and 101(a).

As well as in the stable cases with constant X/R ratio presented in Figures 97 and 98, the current waveforms follow their setpoints prior, during and after the perturbation. As the voltage signals do, they show a transient peak period that lasts until the perturbation is settled down to the step value of 1.01 p.u, at the beginning and at the end of the perturbation.

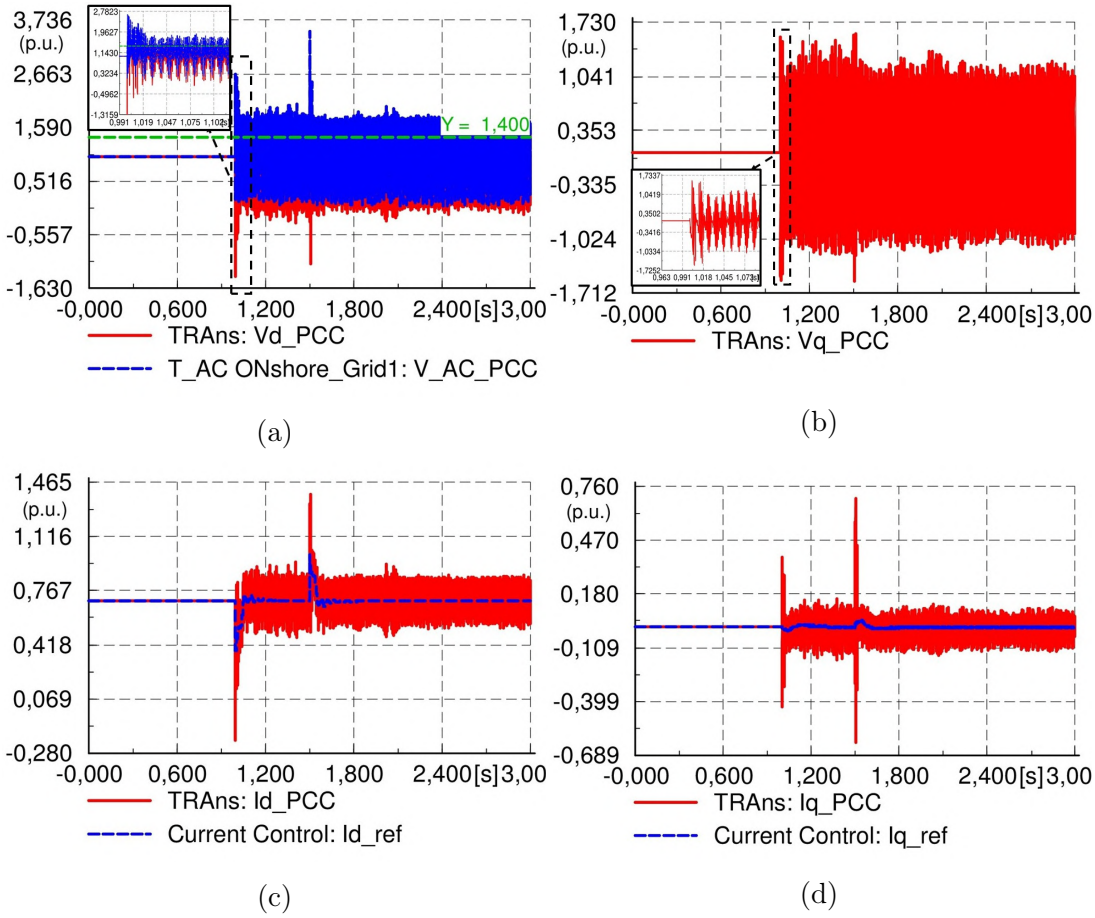

Figure 100: Verification of an unstable case in a weak AC grid for a -20% variation of X/R: (a) Module of AC voltage measured at the PCC ($V_{AC,PCC}$ (p.u.)) and AC voltage measured at the PCC in d coordinate ($V_{d,PCC}$ (p.u.)), (b) AC voltage measured at the PCC in q coordinate ($V_{q,PCC}$ (p.u.)), (c) Current reference for d coordinate ($I_{d,ref}$) and current measured at the PCC in d coordinate ($I_{d,PCC}$) and (d) Current reference for q coordinate ($I_{q,ref}$) and current measured at the PCC in q coordinate ($I_{q,PCC}$).

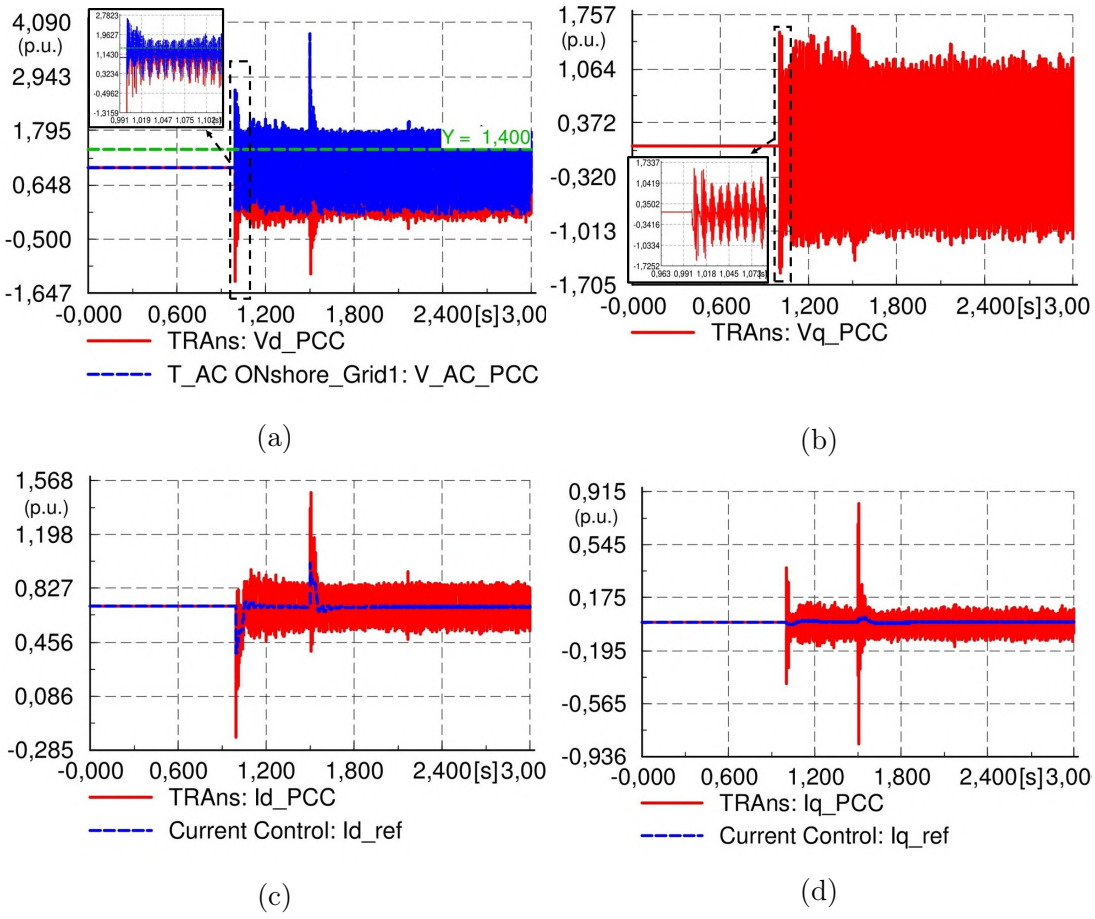

Figure 101: Verification of an unstable case in a weak AC grid for a -10% variation of X/R: (a) Module of AC voltage measured at the PCC ($V_{AC,PCC}$ (p.u.)) and AC voltage measured at the PCC in d coordinate ($V_{d,PCC}$ (p.u.)), (b) AC voltage measured at the PCC in q coordinate ($V_{q,PCC}$ (p.u.)), (c) Current reference for d coordinate ($I_{d,ref}$) and current measured at the PCC in d coordinate ($I_{d,PCC}$) and (d) Current reference for q coordinate ($I_{q,ref}$) and current measured at the PCC in q coordinate ($I_{q,PCC}$).

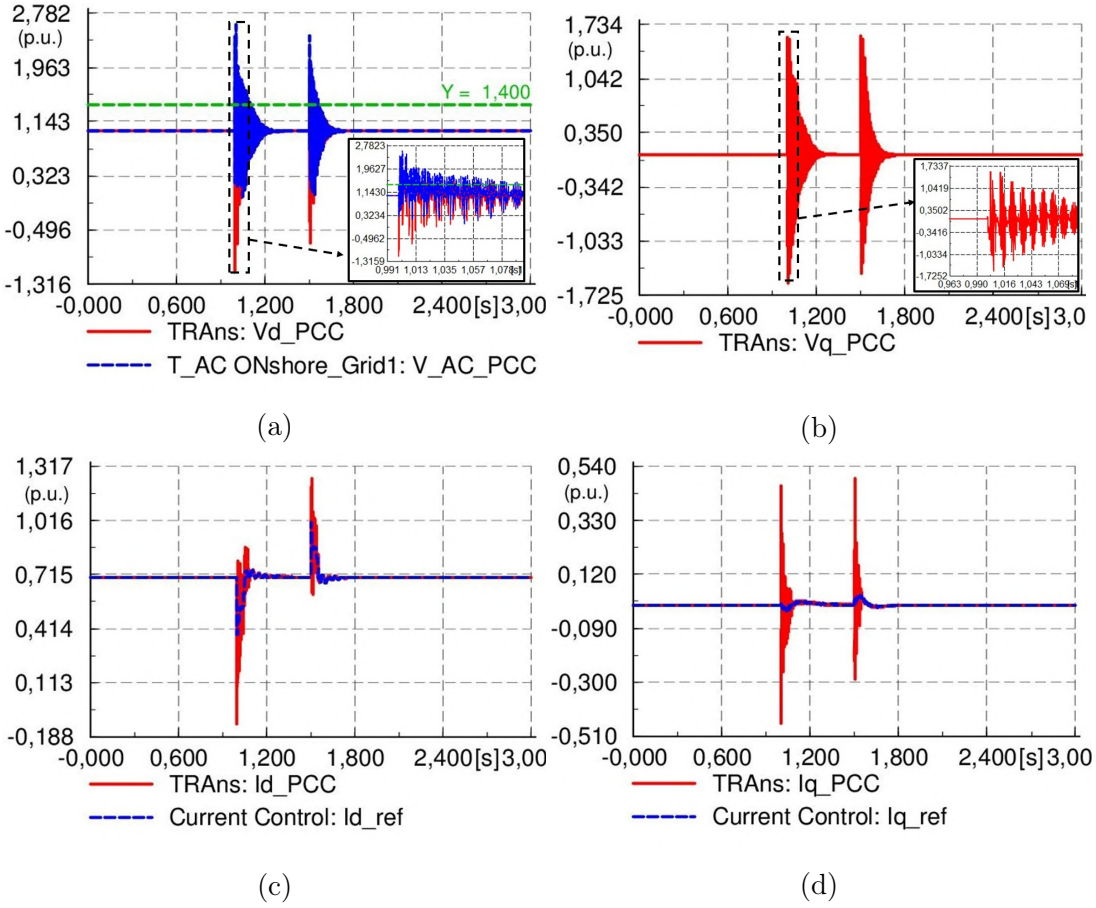

Figure 102: Verification of a stable case in a weak AC grid for a +10% variation of X/R: (a) Module of AC voltage measured at the PCC ($V_{AC,PCC}$ (p.u.)) and AC voltage measured at the PCC in d coordinate ($V_{d,PCC}$ (p.u.)), (b) AC voltage measured at the PCC in q coordinate ($V_{q,PCC}$ (p.u.)), (c) Current reference for d coordinate ($I_{d,ref}$) and current measured at the PCC in d coordinate ($I_{d,PCC}$) and (d) Current reference for q coordinate ($I_{q,ref}$) and current measured at the PCC in q coordinate ($I_{q,PCC}$).

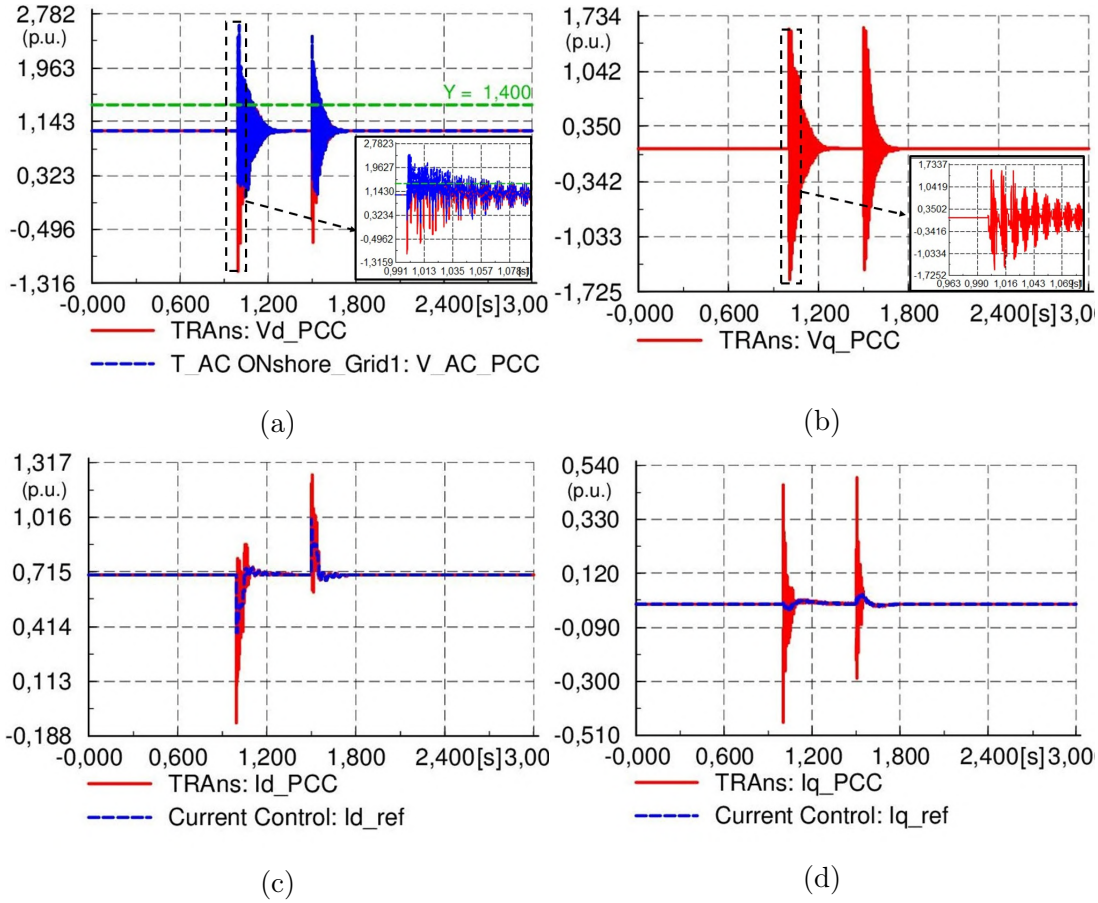

Figure 103: Verification of a stable case in a weak AC grid for +20% variation of X/R: (a) Module of AC voltage measured at the PCC ($V_{AC,PCC}$ (p.u.)) and AC voltage measured at the PCC in d coordinate ($V_{d,PCC}$ (p.u.)), (b) AC voltage measured at the PCC in q coordinate ($V_{q,PCC}$ (p.u.)), (c) Current reference for d coordinate ($I_{d,ref}$) and current measured at the PCC in d coordinate ($I_{d,PCC}$) and (d) Current reference for q coordinate ($I_{q,ref}$) and current measured at the PCC in q coordinate ($I_{q,PCC}$).

5.5 Verification of solutions to an unstable case

In this section, the solutions to the unstable case derived from the deviation of X/R ratio into a -20% from its usual value are hereafter proved by EMT simulations. According to section 4.2.3 of chapter 4, two types of solutions were suggested to bring the system back to stability again, whenever the X/R ratio deviated by a -20% from its usual value.

1. *The increase of k_p from 1.5 to 1.65.*

2. *The reduction of k_i from 30000 to 25000.*

The solutions based on the modification of k_p and k_i are verified by means of Figures 109 and 105, respectively. In both cases, the voltage signals present a transient oscillatory period that decreases progressively until they reach the steady-state value, as shown in the zoomed areas in Figure 104(a),104(b), 105(a) and 105(b).

However, as predicted by the analysis conducted in section 4.2.3 of chapter 4, the transient oscillations of the solution based on k_i change present lower amplitude than those provoked by the solution based on k_p change.

In both solutions, the current signals at PCC follow their setpoints during the whole simulation time, as shown in Figure 104(c), 104(d), 105(c) and 105(d).

A fact that may draw the attention in the verification graphs is that $V_{d,PCC}$ presents negative values during transient peaks, even in stable cases. However, as long as $V_{AC,PCC}$ does not become negative, $V_{d,PCC}$ may reach a negative range due to trigonometric operations that conform the Park transformation and therefore, this fact does not imply any risk of instability.

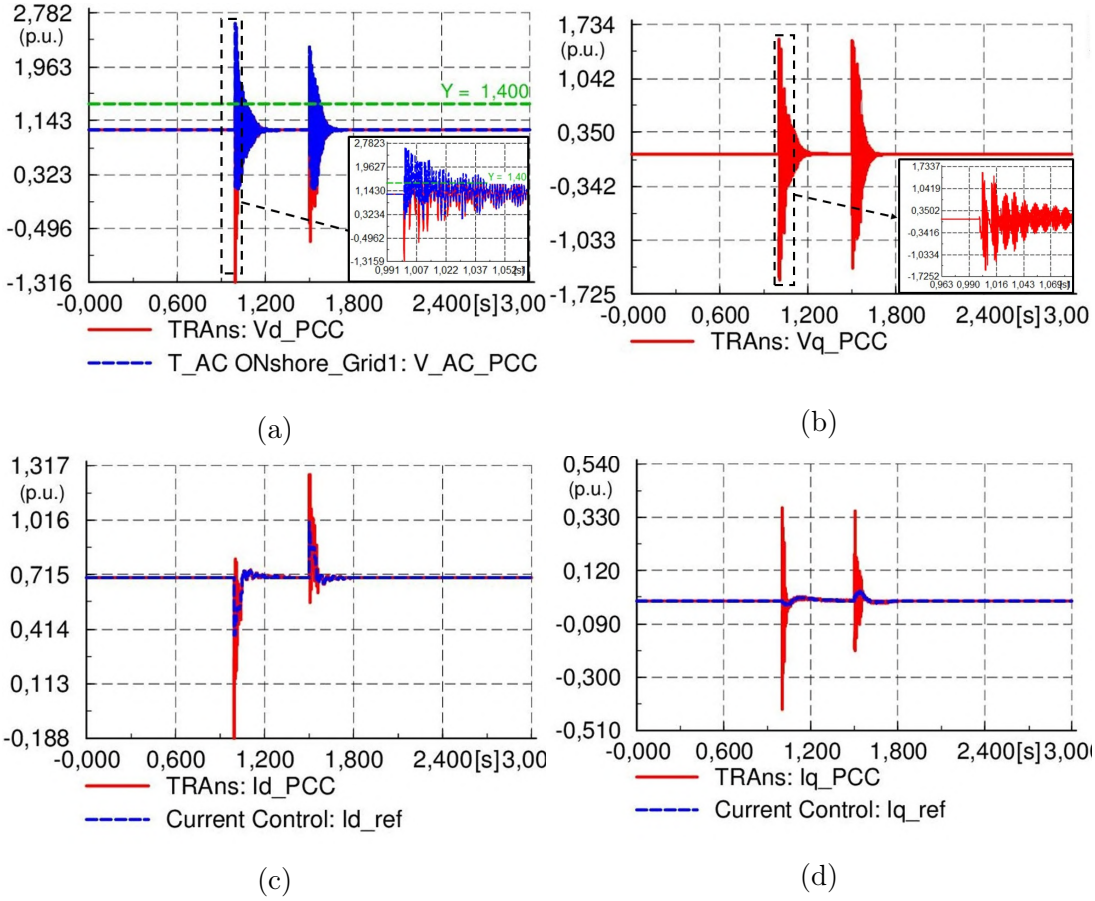

Figure 104: Verification of the solution based on the change in k_p to 1.65 in a weak AC grid for -20% variation of X/R: (a) Module of AC voltage measured at the PCC ($V_{AC,PCC}$ (p.u.)) and AC voltage measured at the PCC in d coordinate ($V_{d,PCC}$ (p.u.)), (b) AC voltage measured at the PCC in q coordinate ($V_{q,PCC}$ (p.u.)), (c) Current reference for d cooordinate ($I_{d,ref}$) and current measured at the PCC in d coordinate ($I_{d,PCC}$) and (d) Current reference for q cooordinate ($I_{q,ref}$) and current measured at the PCC in q coordinate ($I_{q,PCC}$).

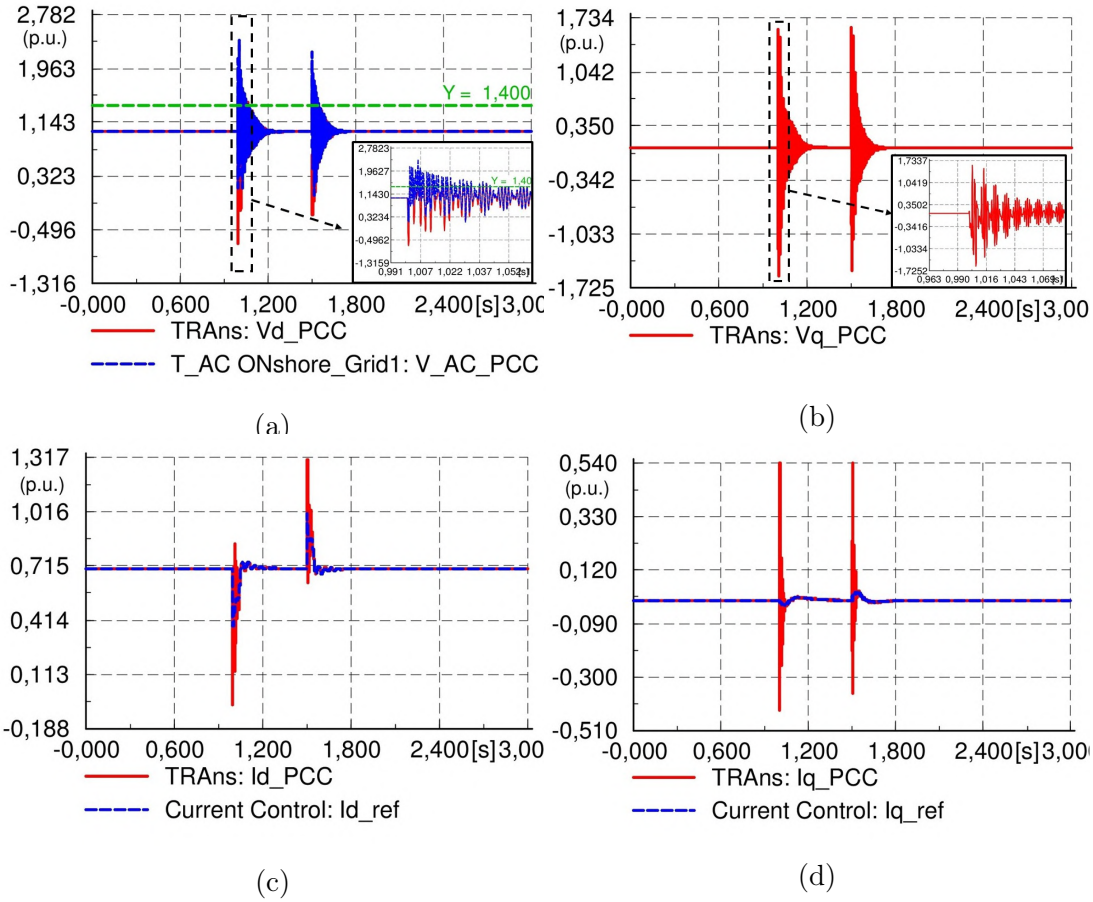

Figure 105: Verification of the solution based on the change in k_i to 25000 in a weak AC grid for -20% variation of X/R: (a) Module of AC voltage measured at the PCC ($V_{AC,PCC}$ (p.u.)) and AC voltage measured at the PCC in d coordinate ($V_{d,PCC}$ (p.u.)), (b) AC voltage measured at the PCC in q coordinate ($V_{q,PCC}$ (p.u.)), (c) Current reference for d coordinate ($I_{d,ref}$) and current measured at the PCC in d coordinate ($I_{d,PCC}$) and (d) Current reference for q coordinate ($I_{q,ref}$) and current measured at the PCC in q coordinate ($I_{q,PCC}$).

5.6 Justification of the methodological process

The methodological process has been verified by means of EMT simulations in DIgSILENT PF, showing coherence with the eigenvalue trajectory analysis conducted in section 4.2 of chapter 4. However, several remarks must be emphasised to analyse the limits of the methodology and confront it with other recent studies.

As for the conclusions derived from the methodology, the fact that the unstable cases arise in weak AC grids for reductions and not increments of X/R characteristic, can be justified by other complementary studies in the literature. The author of [36] claims that weak AC grids suffer significant parameters variation with the change of SCR and/or X/R ratios. According to [36, 116], a decrease in X/R ratio, which makes the AC system more resistive, provokes that the AC voltage oscillate more as the active power transfer changes. In this situation, the reactive power export capability increases, which does not contribute to maintain the AC voltage at the PCC either. Apart from this, the study in [72] also concludes that low X/R ratios increase the step-voltage variations at the PCC of a wind farm connected to a distribution system. Consequently, oscillatory spikes induced in the AC voltage at the PCC risk the stability of the system.

The methodology proposed by the present PhD thesis serves the purpose of extracting implications for tuning PR controlled VSCs, when facing changes in SCR and X/R variations for which the stability is lost. Besides, by means of the tuning strategies based on the either the increase of k_p and/or the decrease of k_i, the system can become stable again. It must be remarked that the changes in k_p and k_i suggested by the two types of solutions are large enough to drive the system back to the stable region, but do not account for the exact limits beyond which the stability is achieved or lost. This consideration has been adopted due to differences between the small signal model and the EMT model, namely 0.038 % of relative error in the worst-case scenario. These differences are mainly due to linearisations, the presence of additional elements neighbouring the domain under study in the original application that are absent in the small signal model and the absence of PLL model in the small signal system. And they cause the slight displacement of the actual boundary k_p and k_i values used in the small signal, compared to those used in the EMT model, though the tendency and conclusions are anyway supported by the EMT model.

There are research centres that opt for verification techniques via software to check the results of the stability analysis, since their software platforms are provided with models with enough level of detail. However, although the present methodology has been verified via EMT simulations in DIgSILENT PF with an

accuracy of 6 decimal places, a more detailed model for VSC could have been implemented in the verification process. Besides, an experimental setup could add new interesting perspectives on the final implications of the methodology.

5.7 Summary

In this chapter the main cases extracted in the methodology have been verified by means of EMT simulations conducted in DIgSILENT PF, against a perturbation in DC voltage setpoint of 1% of its steady-state value. Besides, several aspects of the EMT simulations are further discussed and the main implications for tuning PR controllers have been justified considering other research studies that have been previously published.

6 Conclusions and future work

6.1 Conclusions

This PhD thesis has investigated the small signal stability of a PR- controlled VSC connected to an AC system when subjected to reductions of SCR to weak values while, on the one hand, X/R is constant, and on the other hand, X/R deviates from its usual value.

The progressive weakening of AC networks with the massive integration of RES has been widely reported in the recent literature and these scenarios also contribute to test this phenomenon. Therefore, VSC controllers must be designed and tuned according to these emergent variations that are occurring nowadays more and more frequently. However, the author of this PhD thesis has found that the impact of X/R ratio on the small signal stability of VSC-AC systems has been underestimated in the recent literature.

The effect of combined changes in SCR and X/R ratio challenges the design and tuning of outer and inner loop controllers of VSC and sheds light on cases where the PR controller was well tuned for a weak AC grid scenario, but it loses stability for a specific variation of X/R characteristic.

The methodology presented in this PhD thesis has used the state-space representation to construct a small signal model of the domain under study. For this purpose, a small signal model per each subsystem of the whole domain under study has been built. These small signal models have been validated first separately and then connected into a complete closed-loop system. The closed-loop small signal model has been validated by means of three perturbation cases conducted in an EMT model in DIgSILENT PF, which have encompassed deviations in DC and AC voltage setpoints and reactive power. The comparison of responses coming from the small signal model and the EMT model showed enough accuracy by the small signal model side with a relative error of 0.038 % in the worst-case scenario. This relative error encompasses the differences between the two models due to the linearisation process, the absence of PLL in the small signal model and several neighbouring elements that surround the domain under study in the EMT model, which are not included in the small signal model. These aspects provoke small variations on the steady-state point and slightly distort the transient peaks. Although DIgSILENT PF provides an accuracy of 6 decimal places, an experimental validation would add reliability to the study.

Apart from this, being PR control one of the main cores of this PhD thesis, different topologies of PR controller have been analysed and compared with each other, in terms of their advantages and disadvantages. For the sake of simplicity, an ideal topology has been chosen without considering complementary feedback branches or harmonic filtering. Nevertheless, the small signal model of this type of controller poses additional modelling difficulties, in comparison to its alternative PI controller. Since the scheme of PR operates in $\alpha\beta$ coordinates, it must be converted into dq frame in order to be connected to the remaining dq system. The remaining system operates in dq coordinates since the outer loop of the VSC studied in this PhD thesis is made of PI controllers. The conversion from $\alpha\beta$ to dq coordinates requires the inclusion of a modulation stage which is translated into summing a $j\omega$ to each s term. Such operation implies the arising of coupling terms, the increment of the polynomial order and along with this, the generation of new state variables. A small signal equivalent for the PR controller has been generated considering three state variables per axis, amounting to six in contrast to only four state variables that the PI requires. In return, the PR controller scheme provides an increased functionality in terms of stability and dynamic response, with respect to PI controller. However, other PR control schemes different from the ideal PR topology could have also been tested, as well as, several functionalities, such as the harmonic filtering, that could have been implemented within the specific PR controller scheme.

The PR controller has been tuned in the beginning with a PR parameterisation that provides enough stability margin. However, this parameterisation could have also considered the design of VSC output filter, which has been left unmodified along the study. The outer loop has been tuned in order to give an adequate DC voltage response, not surpassing a 7.5% of overshoot and by having a time response limited by 100 ms. With these baseline parameterisations, the small signal model has been used to carry out the eigenvalue analysis.

In the first place, the stiffness of the AC grid to which the VSC is connected has been varied when the X/R characteristic is constant. For such variation, the trajectory of eigenvalues has been obtained. Hence, a range of k_p and k_i values has also been tested for stiff and weak AC grid scenarios. In a stiff AC grid, the decrease of k_p and/or the increase of k_i move the eigenvalues within the stable region but towards the imaginary axis, so that they progressively reduce the stability margins. Besides, the decrease of k_p to low values in a weak AC grid has been proven to drive the system to instability, while k_i does not present very significant influence.

In the second place, the eigenvalue trajectories have been obtained for variations of X/R characteristic in a weak AC grid, for the baseline PR parameterisation. The purpose of this analysis has been to address the sensitivity of the stability of the system to ±10% and ±20% changes in the X/R ratio for a given PR parameterisation and a weak AC grid scenario. According to the analysis conducted in chapter 4, several unstable cases have been identified in weak AC grids with lowered X/R characteristic from their usual value. With a view to address these issues, the methodology proposes new tuning strategies based on the modifications of k_i and k_p values. The analysis concludes that either the increase of k_p and/or the decrease of k_i can return the system back to stability again. Moreover, the strategy based on the reduction of k_i also diminishes the oscillatory component of the critical eigenvalues.

As for the new tuning strategies, it seems obvious that the modification of the proportional constant of PR controller is the way of driving the system back to stability again in weak AC grids, which typically present poor stability margins. However, the X/R characteristic has not been included in the studies of SCR reductions so far. Therefore, though not being the newest strategy, it yields to the conclusion that the k_p range to guarantee the stability of a critically stable system is displaced when X/R ratio is altered from its usual value.

Apart from this and being this methodology aimed at checking instabilities for low levels of X/R ratio modifications, the displacements of the eigenvalues crossing the imaginary axis are very limited. Consequently, the absolute real positive coordinates for unstable eigenvalues are very close to the coordinate origin. However, cases with larger variation on X/R ratio have also been checked with similar conclusions, though these large changes in the X/R ratio of the AC grid have not been reported yet. Anyway, for larger variations of the X/R ratio the displacement of the eigenvalues along the real axis would be increased.

The previous conclusions have also been verified against EMT simulations carried out in DIgSILENT PF. It must be remarked that the changes in k_p and k_i suggested by the two types of strategies are large enough to drive the system back to the stable region, but do not account for the exact limits beyond which the stability is achieved or lost. This consideration has been adopted due to the small relative error of 0.038 % between the small signal model and the EMT model.

In previous chapters, the unstable cases have been interpreted and contextualised with phenomena occurring in the AC networks. Weak AC grids suffer significant parameters variation with the change of SCR and/or X/R ratios. Apart from

this, reductions in the X/R ratio make the AC system more resistive, provoking the arising of AC voltage oscillations as the active power transfer changes. In this situation, the reactive power export capability increases, which does not contribute to maintain the AC voltage at the PCC either. The arising of voltage spikes happens especially in AC grids with low values of SCR and X/R ratio and turn to risk the stability.

The whole analysis clearly shows that not only the stiffness of the AC grid must be considered in order to tune the PR controlled VSCs, but also the X/R characteristic in order to completely assess the risk of the VSC-AC system to instabilities. The validity of this methodology, and therefore, the findings can also be extended to an MMC under the assumption of CM control, as detailed in section 3.4 of chapter 3.

As a result of the development of the PhD thesis, the following contributions have been made.

- *Development of a methodological tool or guideline to identify unexpected small signal instability issues of a VSC connected to an AC grid.* The methodological approach proposed by this PhD thesis can help researchers when trying to identify sources of unexpected instabilities in a system.

- *Identification of weak AC grid scenarios that with the change of X/R characteristic compromise and lose the stability.* So far, small signal stability studies in weak AC grids have considered the reduction of SCR values but not combined with slight modifications in X/R ratio. These scenarios have been found through a deep review in the literature. Besides, the scenarios and conclusions of the present work may help grid code makers when defining local connection requirements of VSCs.

- *Development of a methodology which extracts implications for tuning PR current controlled VSCs connected to AC grids with variable strength and X/R ratio.* For this purpose, a small signal model of a PR controlled VSC connected to an AC grid has been constructed and numerically validated. A systematic procedure for eigenvalue trajectory analysis is proposed to address the variable X/R characteristic of the AC grid. Besides, the cases extracted from the methodology have been verified by EMT simulations, and the methodology has been justified to be extended to modular multilevel converters under the compensated modulation control approach.

6.2 Future work

This thesis has addressed the tuning criteria of PR controlled VSCs when subjected to combined changes of SCR and X/R ratios of the AC grid to which is connected. Being this a finite work, there are future lines that can continue the work initiated by this thesis.

- *The AC grid model, defined by its Thevenin equivalent, could be a more detailed one, such as a synchronous generator.* In this case, the eigenvalue analysis could also take into account other variables related to the control and dynamics of a synchronous generator, in order to study more complex resonances of the system and extract more complete criteria for tuning control parameters in order to avoid such risk of resonances. Besides, the effect of the DC grid current dynamics could be also included in the study, as well as the presence of a capacitive element in the VSC output filter.

- *As for the MMC context, the application of the methodology could be extended to MMCs driven by control structures that do not follow the CM control approach.* For these cases, more detailed models of converters and other components could be simulated.

- *The studied system could also be connected to a grid with more VSCs, AC lines and synchronous generators*, in order to study more complex interactions.

- *The methodology could be tested in applications where other PR controller schemes are implemented.* Different PR control schemes, according to feedback branches and/or harmonic filtering, could also be compared in terms of minimising the risk of instability originated by changes in SCR and X/R ratio.

- *The methodology could be applied to other power grid contexts where the change in X/R ratio is more frequent, such as the electrical distribution context or microgrids.* Therefore, the methodology proposed by this PhD thesis could also be applied to this context by making the necessary and pertinent adaptations.

- *An experimental setup could also be used to carry out additional validation process of the methodology.* This would give the new perspectives to the implications of the methodology.

Appendix A- Analytical methods for stability analysis

This appendix is aimed at providing a description of the mainly used analytical methods for modelling and analysing the stability of electrical power systems.

Based on the scheme presented in Figure 3, the methods are grouped according to their reference domain, that can lead to either time or frequency-based formulations. The methods within each category are described by means of equations and theorems, and their differences further discussed.

A.1 Time based formulations

Inside this category, two common time-based formulations are presented and described, the state-space representation and the Lyapunov theory. Time-based analytical formulations are validated against numerical simulations by comparing their time responses against the same perturbation.

A.1.1 State-space representation

The state-space theory of time-invariant systems is hereafter presented, according to [115]. The state-space representation of a time-invariant system can be given by a set of non-linear first order ordinary differential equations defined by (70), (71) and (72).

$$\frac{d}{dt}x = f(x,u) \tag{70}$$

$$y = g(x,u) \tag{71}$$

$$x = \begin{pmatrix} x_1 \\ x_2 \\ \vdots \\ x_n \end{pmatrix} u = \begin{pmatrix} u_1 \\ u_2 \\ \vdots \\ u_m \end{pmatrix} f = \begin{pmatrix} f_1 \\ f_2 \\ \vdots \\ f_n \end{pmatrix} y = \begin{pmatrix} y_1 \\ y_2 \\ \vdots \\ y_o \end{pmatrix} g = \begin{pmatrix} g_1 \\ g_2 \\ \vdots \\ g_o \end{pmatrix} \tag{72}$$

In (70),(71) and (72) x represents the state vector composed by n state variables which account for the state of the system, u is a column vector which includes the system inputs, y is a column vector that contains the system output, and f and g are vectors of n and m non-linear functions, respectively. The state-space representation is not unique and several sets of state variables can be used to describe the system.

The x state vector must be composed by n linearly independent systems, so that they encompass the minimum information about the system at every time instant. Both the x state vector and the u input vector determine the behaviour of the system for every time instant. The y output vector gives the responses of the system as a function of the x state variables and u inputs.

Being (70) and (71) usually non-linear expressions, they must be linearised around an operating point, in order to carry out small signal stability analysis.

The process of linearisation starts by defining this specific operating point. The given operating point can be defined by its state and input vectors, x_0 and u_0 and the equilibrium condition, as shown in (73).

$$\frac{d}{dt}x_0 = f(x_0, u_0) = 0 \tag{73}$$

Having defined the equilibrium condition in (73), the state vector x suffers a Δx perturbation, so that the state vector is now updated as $x{=}x_0{+}\Delta x$. Therefore, (70) gets also modified as (74) shows.

$$\frac{d}{dt}x = \frac{d}{dt}x_0 + \frac{d}{dt}\Delta x = f(x_0 + \Delta x, u_0 + \Delta u) \tag{74}$$

Due to the small magnitude of the perturbation, the first order Taylor's series expansion can be used to approximate Δx in (74), as shown in (75), where the terms involving second and higher order powers of Δx and Δu have been neglected.

$$\frac{d}{dt}\Delta x = \frac{\partial f}{\partial x_1}\Delta x_1 + \ldots + \frac{\partial f}{\partial x_n}\Delta x_n + \frac{\partial f}{\partial u_1}\Delta u_1 + \ldots + \frac{\partial f}{\partial u_m}\Delta u_m \tag{75}$$

The modification of state variables given by $x{=}x_0{+}\Delta x$ also affects the output vector by having $y{=}y_0{+}\Delta y$, where Δy can be expressed as (76) shows.

$$\Delta y = \frac{\partial g}{\partial x_1}\Delta x_1 + \ldots + \frac{\partial g}{\partial x_n}\Delta x_n + \frac{\partial g}{\partial u_1}\Delta u_1 + \ldots + \frac{\partial g}{\partial u_m}\Delta u_m \tag{76}$$

If (75) and (76) are expanded into their vector components, the system defined by (70), (71) and (72) is transformed into the equations defined by (77) and (78).

$$\frac{d}{dt}\begin{pmatrix}\Delta x_1\\ \Delta x_2\\ \vdots\\ \Delta x_n\end{pmatrix} = \begin{pmatrix}\frac{\partial f_1}{\partial x_1} & \cdots & \frac{\partial f_1}{\partial x_n}\\ \vdots & \ddots & \vdots\\ \frac{\partial f_n}{\partial x_1} & \cdots & \frac{\partial f_n}{\partial x_n}\end{pmatrix}\begin{pmatrix}\Delta x_1\\ \Delta x_2\\ \vdots\\ \Delta x_n\end{pmatrix} + \begin{pmatrix}\frac{\partial f_1}{\partial u_1} & \cdots & \frac{\partial f_1}{\partial u_m}\\ \vdots & \ddots & \vdots\\ \frac{\partial f_n}{\partial u_1} & \cdots & \frac{\partial f_n}{\partial u_m}\end{pmatrix}\begin{pmatrix}\Delta u_1\\ \Delta u_2\\ \vdots\\ \Delta u_m\end{pmatrix} \tag{77}$$

$$\begin{pmatrix} \Delta y_1 \\ \Delta y_2 \\ \vdots \\ \Delta y_o \end{pmatrix} = \begin{pmatrix} \frac{\partial g_1}{\partial x_1} & \cdots & \frac{\partial g_1}{\partial x_n} \\ \vdots & \ddots & \vdots \\ \frac{\partial g_o}{\partial x_1} & \cdots & \frac{\partial g_o}{\partial x_n} \end{pmatrix} \begin{pmatrix} \Delta x_1 \\ \Delta x_2 \\ \vdots \\ \Delta x_n \end{pmatrix} + \begin{pmatrix} \frac{\partial g_1}{\partial u_1} & \cdots & \frac{\partial g_1}{\partial u_m} \\ \vdots & \ddots & \vdots \\ \frac{\partial g_o}{\partial u_1} & \cdots & \frac{\partial g_o}{\partial u_m} \end{pmatrix} \begin{pmatrix} \Delta u_1 \\ \Delta u_2 \\ \vdots \\ \Delta u_m \end{pmatrix} \tag{78}$$

Equations (77) and (78) are the space-state equations that describe the performance of the small signal system. In order to introduce the state-space matrices, these expressions can be reformulated as indicated in (79) and (80).

$$\frac{d}{dt} \begin{pmatrix} \Delta x_1 \\ \Delta x_2 \\ \vdots \\ \Delta x_n \end{pmatrix} = A \begin{pmatrix} \Delta x_1 \\ \Delta x_2 \\ \vdots \\ \Delta x_n \end{pmatrix} + B \begin{pmatrix} \Delta u_1 \\ \Delta u_2 \\ \vdots \\ \Delta u_m \end{pmatrix} \tag{79}$$

$$\begin{pmatrix} \Delta y_1 \\ \Delta y_2 \\ \vdots \\ \Delta y_o \end{pmatrix} = C \begin{pmatrix} \Delta x_1 \\ \Delta x_2 \\ \vdots \\ \Delta x_n \end{pmatrix} + D \begin{pmatrix} \Delta u_1 \\ \Delta u_2 \\ \vdots \\ \Delta u_m \end{pmatrix} \tag{80}$$

In (79) and (80) the state-space matrices are first introduced: being A the state matrix, B the control matrix, C the output matrix and D the feed-forward matrix. These matrices are given by (81) and (82).

$$A = \begin{pmatrix} \frac{\partial f_1}{\partial x_1} & \cdots & \frac{\partial f_1}{\partial x_n} \\ \vdots & \ddots & \vdots \\ \frac{\partial f_n}{\partial x_1} & \cdots & \frac{\partial f_n}{\partial x_n} \end{pmatrix}; B = \begin{pmatrix} \frac{\partial f_1}{\partial u_1} & \cdots & \frac{\partial f_1}{\partial u_m} \\ \vdots & \ddots & \vdots \\ \frac{\partial f_n}{\partial u_1} & \cdots & \frac{\partial f_n}{\partial u_m} \end{pmatrix} \tag{81}$$

$$C = \begin{pmatrix} \frac{\partial g_1}{\partial x_1} & \cdots & \frac{\partial g_1}{\partial x_n} \\ \vdots & \ddots & \vdots \\ \frac{\partial g_o}{\partial x_1} & \cdots & \frac{\partial g_o}{\partial x_n} \end{pmatrix}; D = \begin{pmatrix} \frac{\Delta g_1}{\partial u_1} & \cdots & \frac{\partial g_1}{\partial u_m} \\ \vdots & \ddots & \vdots \\ \frac{\partial g_o}{\partial u_1} & \cdots & \frac{\partial g_o}{\partial u_m} \end{pmatrix} \tag{82}$$

The stability of a linear system depends merely on the characteristics of the system, regardless of the inputs. Therefore, the state matrix (A) is of special relevance for small signal stability analysis as it contains the characteristics of the system. The stability assessed according to this method is based on the

observation of the responses (y) and the state variables (x) of the system under several perturbations. If the responses and state variables converge to the set-point once the transitory period has passed, then the system is stable. On the contrary, if the responses and the state variables oscillate and do not converge to the setpoint, then the system is unstable.

A.1.2 Lyapunov theory

The following theoretical analysis that describes the Lyapunov theory is based on [117] and [118], which represents an alternate modelling tool to state-space equations.

The ordinary Lyapunov function method evaluates whether a dynamical system is stable or asymptotically stable [118]. In other words, it evaluates whether the system starting in a state in some domain Ω will remain in Ω, or for asymptotic stability will eventually return to x=0. This is introduced by the definition of a dynamic equation given by the state-space equations, as shown in (83).

$$\dot{x} = F(x) \tag{83}$$

Lyapunov's stability theory is based on finding a scalar function $V(x)$ defined in the state-space of the dynamic system described by (83). On the one hand, the Euclidean space determined by x is referred to as the state-space whilst the point x, for which $F(x) = 0$, is referred to as the equilibrium point.

On the other hand, the equilibrium points are also defined as those x for which $\nabla V(x) = 0$. The mathematical condition for checking whether a function $V(x)$ has a maximum or minimum at a stationary point can be derived by obtaining the Taylor series of $V(x)$, as (84) shows, where $H = [\delta^2 V/\delta x_i \delta x_j]$ is the Hessian matrix.

$$V(x + \Delta x) \cong V(x) + \Delta x^T [\nabla V] + \frac{1}{2}\Delta x^T H \Delta x + ... \tag{84}$$

If the function $V(x)$ is subjected to a disturbance $\Delta V(x)$, the increment or reduction in $V(x)$ is shown in (85).

$$\Delta V(x) = V(x + \Delta x) - V(x) \cong \frac{1}{2}\Delta x^T H \Delta x = \sum_{i=1}^{N}\sum_{j=1}^{N} h_{ij}\Delta x_i \Delta x_j \tag{85}$$

In (85) it is shown that the variation in $V(x)$ is equal to the quadratic form of the state variables x_i and x_j, by means of the Hessian matrix $H(x_i, x_j)$.

According to [117], such a quadratic form has a minimum (left-side image in Figure 106) at a given stationary point if, and only if, the Hessian matrix H is positive definite, i.e. that all leading principal minors of the matrix H are positive. In contrast, if all leading principal minors of H are negative then the matrix is negative definite and the quadratic form has a maximum (image in the middle in Figure 106) at a given stationary point. If some leading principal minors are positive and some are negative, the matrix H is non-definite and the quadratic form has a saddle point (right-side image in Figure 106) at the stationary point.

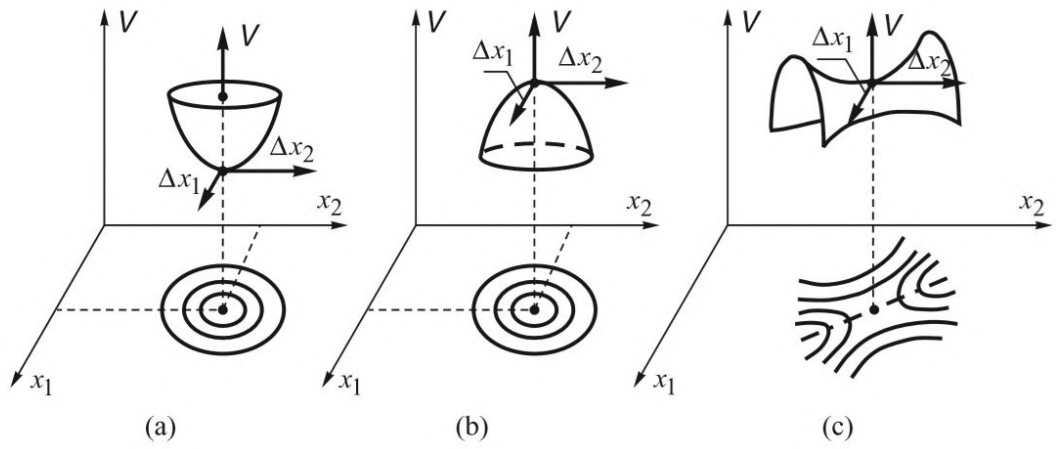

Figure 106: A scalar function of two variables with three types of stationary points: minimum, maximum and saddle point [117].

With the definition of the scalar function $V(x)$ in the state-space, each point on the system trajectory $x(t)$ corresponds to a value of $V(x(t))$. The rate of change of $V(x)$ along the system trajectory $x(t)$ can be expressed as in (86).

$$\dot{V} = \frac{dV}{dt} = \frac{\delta V}{\delta x_1}\frac{dx_1}{dt} + \frac{\delta V}{\delta x_2}\frac{dx_2}{dt} + ... + \frac{\delta V}{\delta x_n}\frac{dx_n}{dt} = [\nabla V(x)]^T \dot{x} = [\nabla V(x)]^T F(x) \quad (86)$$

If a positive definite scalar function $V(x)$ is assumed to have a stationary point at the equilibrium point, any disturbance $\Delta x = 0$ will move the system trajectory to an initial point $x_0 \neq x$.

If the system is asymptotically stable, as seen in Figure 107a, then the trajectory $x(t)$ will tend towards the equilibrium point and $V(x)$ will decrease along the trajectory until $x(t)$ settles at the minimum point.

If the system is unstable, as noted in Figure 107b, then the trajectory will move away from the equilibrium point and $V(x)$ will increase along the trajectory.

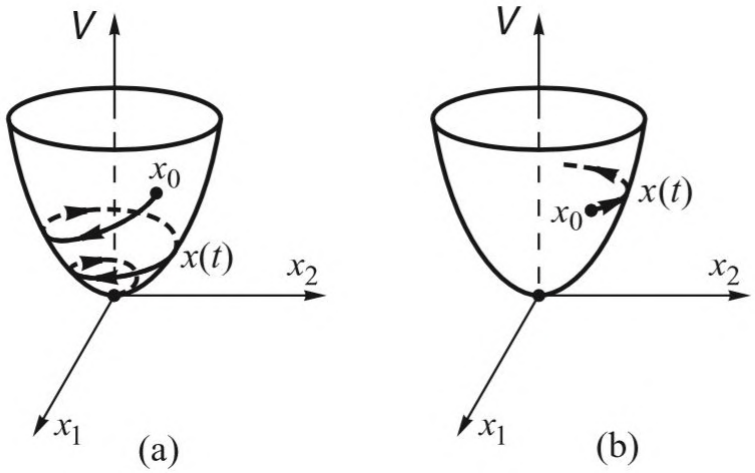

Figure 107: Illustration of Lyapunov's theorems on stability: (a) asymptotic stability and (b) instability [117].

Finally, the main considerations of Lyapunov's theory can be summarised in the following theorem.

Let x be an equilibrium point of a dynamic system $\dot{x} = F(x)$. Point x is stable if there is a continuously differentiable positive definite function $V(x)$, such that $\dot{V(x)} \leq 0$. Point x is asymptotically stable if $\dot{V(x)} < 0$.

One of the main advantages of Lyapunov's theorem is that it can be used to evaluate the stability of a system without deriving and solving differential equations defined by (83) and as the state-space equations require.

However, its drawback is how to find a suitable positive definite Lyapunov function $V(x)$ without determining the system trajectory and for which the sign of the derivative $V(x)$ can be determined. Generally, the Lyapunov function $V(x)$ will be non-linear and may have more than one stationary point.

A.2 Frequency based formulations

The most common frequency-based formulations are hereupon described, namely the eigenvalue analysis and the impedance analysis. Frequency analytical formulations can be verified either comparing the Bode diagrams with those obtained with numerical methods or directly verified by numerical time domain simulations.

A.2.1 Eigenvalue analysis

Eigenvalues and eigenvectors characterise the dynamic evolution of the state variables of a system with the time. The definition of eigenvalues and eigenvectors is hereafter given [115].

The eigenvalues (λ) of the state matrix A are a set of complex numbers for which the following system of equations meet Φ=0, according to (87), where A is the state matrix of nxn dimensions and Φ is a column vector with n rows called right eigenvector.

$$A\Phi = \lambda\Phi \tag{87}$$

The expression in (87) is equivalent to (88), which is known as the characteristic equation of the system and being I the identity matrix.

$$det(A - \lambda I) = 0 \tag{88}$$

The set of n solutions λ_1, $\lambda_2 ... \lambda_n$ of the characteristic equation (88) are the eigenvalues of the system. For each eigenvalue λ_1, $\lambda_2 ... \lambda_n$ it is possible to define an associated right eigenvector Φ_i, defined by (89), that satisfies (87).

$$A\Phi_i = \lambda_i\Phi_i, \forall i = 1, 2, ..., n; \Phi_i = \begin{pmatrix} \Phi_1 \\ \Phi_1 \\ \vdots \\ \Phi_n \end{pmatrix} \tag{89}$$

In (89), Φ_i is the i_{th} right eigenvector with n rows. Besides, a system characterised by an nxn A state matrix has n right eigenvectors that can be grouped as a nxn matrix, as (90) indicates.

$$R = \begin{pmatrix} \Phi_{11} & \Phi_{12} & \dots & \Phi_{1n} \\ \Phi_{21} & \Phi_{22} & \dots & \Phi_{2n} \\ \vdots & \vdots & \ddots & \vdots \\ \Phi_{n1} & \Phi_{n2} & \dots & \Phi_{nn} \\ \end{pmatrix} \tag{90}$$

Alternatively, for every eigenvalue λ_i it is possible to define an associated left eigenvector ψ_i that fulfils (91).

$$\psi_i A = \lambda_i\psi_i, \forall i = 1, 2, ..., n; \psi_i = \begin{pmatrix} \psi_1 & \psi_1 & \dots & \psi_n \end{pmatrix} \tag{91}$$

And analogously to the matrix of right eigenvectors, the matrix of left eigenvectors is built according to (92).

$$L = \begin{pmatrix} \psi_{11} & \psi_{12} & \dots & \psi_{1n} \\ \psi_{21} & \psi_{22} & \dots & \psi_{2n} \\ \vdots & \vdots & \ddots & \vdots \\ \psi_{n1} & \psi_{n2} & \dots & \psi_{nn} \\ \end{pmatrix} \tag{92}$$

Therefore, the right eigenvector matrix (R) and the left eigenvector matrix (L) are related by the expression in (93).

$$L = R^{-1} \tag{93}$$

The expression in (89) is used to calculate the eigenvalues of the system while (89) and (93) are used to calculate the eigenvectors.

If the inputs of the system are set to zero, then (79) takes the form of (94).

$$\frac{d}{dt} \begin{pmatrix} \Delta x_1 \\ \Delta x_2 \\ \vdots \\ \Delta x_n \end{pmatrix} = A \begin{pmatrix} \Delta x_1 \\ \Delta x_2 \\ \vdots \\ \Delta x_n \end{pmatrix} \tag{94}$$

The solution of (94) for the i-th state variable when the system inputs are zero depend merely on the initial conditions of the state variables, as shown in (95).

$$\begin{gathered} \Delta x_i = \Phi_{i1}(\psi_{11}\Delta x_1(0) + \psi_{12}\Delta x_2(0) + \ldots + \psi_{1n}\Delta x_n(0))e^{\lambda_1 t} + \\ \Phi_{i2}(\psi_{21}\Delta x_1(0) + \psi_{22}\Delta x_2(0) + \ldots + \psi_{2n}\Delta x_n(0))e^{\lambda_2 t} + \\ \dots \\ + \Phi_{in}(\psi_{n1}\Delta x_1(0) + \psi_{n2}\Delta x_2(0) + \ldots + \psi_{nn}\Delta x_n(0))e^{\lambda_n t} \end{gathered} \tag{95}$$

In (95) λ_1,λ_2,...,λ_n are the eigenvalues of the state matrix, $\Delta x_i(0)$ is the initial condition of the i-th state variable and Φ_{xy} and ψ_{xy} the entries of the left and right eigenvalues respectively.

According to (95), the dynamic evolution of state variables is built as the superposition of n dynamic modes, where $e^{\lambda_i t}$ represents the time characteristic of a mode corresponding to a λ_i eigenvalue. The general expression of an eigenvalue

(λ_i) is given by (96), where σ_i and ω_i are the real part and imaginary parts, respectively.

$$\lambda_i = \sigma_i \pm j\omega_i = e^{\sigma t} cos(\omega t + \varphi) \tag{96}$$

Complex eigenvalues appear in conjugate pairs, i.e. $\lambda_i = \sigma_i + j\omega_i$ and $\lambda_i = \sigma_i - j\omega_i$. The combined effect of both conjugate pairs in the dynamic equation of the system has the form expressed in the right term of the expression in (96). Consequently, complex conjugate eigenvalues produce oscillatory modes. The real part of the eigenvalue (σ_i) represents the damping of the mode. If σ_i is negative, the mode is damped and its amplitude falls towards zero with the time. Consequently, the response of the system for that mode is stable. The larger σ_i is, the faster decay of the amplitude is observed. On the other hand, if σ_i is positive, the amplitude of the oscillation increases continuously and the system is unstable.

As for the imaginary component (ω_i) of (96), it represents the damped angular frequency. The corresponding damped frequency is given by (97).

$$f_{d,i} = \frac{\omega_i}{2\pi} = f_{n,i}\sqrt{1 - \zeta_i^2} \tag{97}$$

In the right term of (97), two parameters are introduced: the damping ratio (ζ_i) and the undamped natural frequency (f_n). The damping ratio (ζ_i) represents the rate of decay of the amplitude of the mode and it is given by (98).

$$\zeta_i = \frac{-\sigma_i}{\sqrt{\sigma_i^2 + \omega_i^2}} \tag{98}$$

The damping ratio measures the number of undamped cycles that takes the response to attenuate. According to (96), the amplitude of the mode decays to 1/e or 37% of the initial amplitude in $1/|\sigma_i|$ seconds or in $1/(2\pi\zeta_i)$ cycles of oscillation. As for the undamped natural frequency, ($f_{n,i}$) represents the frequency of oscillation of the mode of an equivalent undamped system, i.e an equivalent system but with $\zeta = 0$.

Therefore, the location of eigenvalues in the complex plane determine the stability of the system and the system's dynamic characteristics as follows.

- *If an eigenvalue is positive* the system becomes unstable, while if it is negative the system is stable.
- *An eigenvalue with just a real part and the imaginary part set to zero ($\omega_i = 0$)* becomes a real eigenvalue, which corresponds to a non-oscillatory mode.

- *The damping ratio and the natural undamped frequency* determine the oscillatory behaviour of the system.

In order to study the influence of the eigenvectors on the dynamics of the state variables, the participation factor theory can be found in [115].

A.2.2 Impedance analysis

While the state-space and eigenvalue analysis require the detailed analytical modelling information for studying the stability, impedance-based small signal stability analysis method does not need the detailed modelling of the system [26].

An impedance model for the power system is analytically derived in an analogous approach as the state-space equations for each subsystem, but considering the impedance model of each subsystem and putting them together, so that they are grouped into two different blocks: the load and the source impedance, as seen in Figure 108.

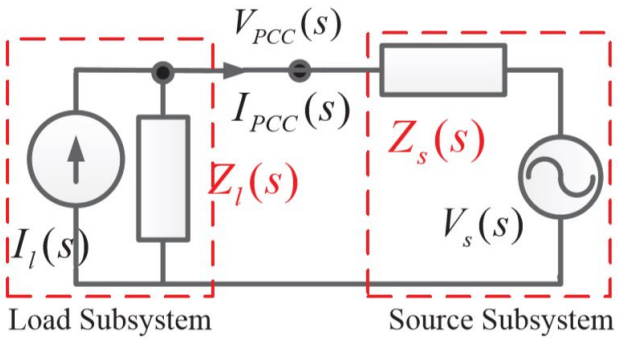

Figure 108: Equivalent impedance model [26].

According to Figure 108, the source subsystem is modelled by its Thevenin equivalent circuit, consisting of an ideal voltage source (V_s) in series with an output impedance (Z_s), while the load subsystem is modelled by its Norton equivalent, composed by an ideal current source (I_l) in parallel to its input impedance (Z_l) [119]. By having the system presented in Figure 108, the current I_{PCC} flowing from the source to the load can be calculated as deduced from (99).

$$I_{PCC}(s) = \frac{V_s(s)}{Z_l(s) + Z_s(s)} = \frac{V_s(s)}{Z_l(s)} * \frac{1}{1 + Z_s(s)/Z_l(s)} \tag{99}$$

The source voltage is assumed to be stable when it is unloaded and the load current when it is powered from an ideal source, which makes both $V_s(s)$ and

$1/Z_l(s)$ stable. Therefore, the stability of the current at the PCC depends on the stability of the term in (100).

$$H(s) = \frac{1}{1 + Z_s(s)/Z_l(s)} \tag{100}$$

According to (100) $H(s)$ adopts the shape of a close-loop transfer function of a negative feedback control system, where the forward gain is 1 and the feedback gain is $Z_s(s)/Z_l(s)$ [119]. The latter is defined as the ratio of the source output impedance to the load input impedance. According linear control theory, $H(s)$ is stable if and only if $Z_s(s)/Z_l(s)$ satisfies the Nyquist stability criterion [120].

According to [120], the Nyquist stability criterion determines the stability of a closed-loop system from its open-loop frequency response and poles. This criterion represents graphically the contour of $Z_s(s)/Z_l(s)$ in the s plane and three possibilities can occur:

- *There is no encirclement of the −1+j0 point* (Figure 109(a)). This implies that the system is stable if there are no poles of $Z_s(s)/Z_l(s)$ in the right half-plane; otherwise, the system is unstable.
- *There are one or more counterclockwise encirclements of the −1+j0 point.* In this case the system is stable if the number of counterclockwise encirclements is the same as the number of poles of $G(s)H(s)$ in the right half-plane; otherwise, the system is unstable.
- *There are one or more clockwise encirclements of the −1+j0 point* (Figure 109(b)). In this case the system is unstable.

Unlike eigenvalue analysis, Nyquist stability criterion can determine the absolute stability of the closed-loop system graphically from open-loop frequency-response curves, without needing to determine the closed-loop poles. Therefore, analytically obtained open-loop frequency-response curves, as well as those experimentally obtained, can be used for the stability analysis. This is convenient because it often happens that mathematical expressions for some of the components are unknown and only their frequency-response data are available.

(a) (b)

Figure 109: Nyquist paths according to stability (a) Stable Nyquist path, with no encirclements of -1+j0 and (b) Unstable Nyquist path, with an encirclement of -1+j0 [120].

A.3 Discussion of methods

Finally, the methods previously described are compared to extract the main advantages and disadvantages of each one with respect to the others.

As for the time-based formulations, the state-space equations are derived and can be linearised by following a common and systematic procedure, but at the cost of requiring detailed information of each subsystem that is not needed in its alternate method, the Lyapunov theory. In the Lyapunov method, the stability of a system can be assessed without deriving and solving the differential equations imposed by the state-space system. However, it requires the effort of obtaining a suitable positive definite scalar function without knowing the system's trajectories and for which its derivative sign can be determined. Therefore, a more complex procedure is involved in Lyapunov theory than in the derivation of state-space equations.

As for the frequency-based formulations, the eigenvalue analysis has the advantage of determining global stability of a system but, as its homologous state-space equations method, it requires very detailed information. The impedance-based analysis does not require such deep level of details since the open-loop poles are sufficient to determine stability of the system. However, impedance-based analysis is generally only valid to assess local stability. In contrast, global stability is used in bigger systems that experiment more complex interactions which imply detailed modelling and thus eigenvalue analysis is preferable for these cases.

Appendix B- EMT model parameters in DIgSILENT PF

In this appendix the main model and control parameters are gathered for each element shown in Figure 71. Names in parentheses correspond to the specific name given in Figure 71.

B.1 General information of each model

Model	Description
AC line model (LineAC_Grid)	Conductor material: Copper Insulation material: PVC Multi-core with non-metallic (PVC) sheath and armoured cable
Onshore and offshore VSC models (Conv_ONshore and Conv_OFFshore)	two-level VSC. Modulation: Sinusoidal VSC model: Controlled Voltage Source
DC line model (DC-Line_pos and DC-Line_neg)	Conductor material: Copper Insulation material: PVC Multi-core with non-metallic (PVC) sheath and armoured cable
Wind park AC line model (LineAC_WPark)	Conductor material: Copper Insulation material: XLPE Multi-core with non-metallic (PVC) sheath and armoured cable
Wind park model (WindPark (SG))	Static generator

Table 5: General configuration of each model in DIgSILENT PF

B.2 AC line model (LineAC_Grid)

Parameter	Description	Value
V_{AC}	Rated AC voltage (kV)	275
I_{AC}	Rated AC current (kA)	2
R	AC line resistance (Ω/km)	0.015
L	AC line inductance (mH/km)	0.4
C	AC line parallel capacitance (μF/km)	0.22
G	Conductance (μS/km)	0
X/R	AC line X/R ratio	8.37
l_{line}	AC line length (km)	1

Table 6: EMT model parameters of AC line model in DIgSILENT PF

B.3 Onshore VSC model (Conv_ONshore)

Parameter	Description	Value
V_{DC}	Rated DC voltage (kV)	640
V_{AC}	Rated AC voltage (kV)	275
S_{VSC}	Rated VSC power (MVA)	560
R_f	VSC output filter (Ω)	0.001
L_f	VSC output filter(H)	0.014
P_{nold}	No load losses (kW) of VSC	4000
$swtLossFactor$	Switching loss factor (kW/A) of VSC	0
Ron	On resistance for diode/transistor parameter (Ω) of VSC	0.0001
$Goff$	Off-conductance (μS) of VSC	0.001
$R0/R1$	R0/R1 ratio of VSC	1
$X0/X1$	X0/X1 ratio of VSC	1
CapONshore	Onshore capacitor (μF)	450

Table 7: EMT model parameters of the onshore VSC model in DIgSILENT PF

B.4 DC line model of the HVDC bipolar configuration (DC-Line_pos and DC-Line_neg)

Parameter	Description	Value
V_{DCline}	Rated DC voltage (kV)	320
I_{DCline}	Rated current (kA) in ground	1.5
R_{DCline}	Resistance (Ω/km)	0.0063
L_{DCline}	Inductance (mH/km)	1.27324
C_{DCline}	Capacitance (μF/km)	0.01
G_{DCline}	Conductance (μS/km)	0
l_{DCline}	Length of DC line (km)	100
–	Derating factor of DC line	1

Table 8: EMT parameters of DC line of the bipolar HVDC configuration in DIgSILENT PF

B.5 Control of onshore VSC

Parameter	Description	Value
ω	Resonant angular frequency-PR control (rad/s)	314.159
k_q	Outer loop control -proportional constant of PI controller in the q axis	0.4
T_q	Outer loop control-time constant of PI controller in the q axis (s)	0.01
k_v	Outer loop control-proportional constant of PI controller in the d axis	30
T_v	Outer loop control-time constant of PI controller in the d axis (s)	0.09
k_{FSM}	Outer loop control-frequency sensitive mode slope	0.05
$k_{droop,AC}$	Outer loop control-droop AC control constant	-2.2
$T_{rV_{DC}}$	Filter time constant-DC Voltage (s)	0.01
T_{rq}	Filter time constant -reactive Power (s)	0.02
dbd	Dead-band droop AC Voltage (p.u.)	0.005
k_p	Inner loop control-proportional constant of PR controller in dq axis	1.5
k_i	Inner loop control-integral constant of PR controller in dq axis (s)	30000

Table 9: Control parameters of onshore VSC model in DIgSILENT PF

B.6 Wind park AC line (LineAC_WPark)

Parameter	Description	Value
$V_{AClineWP}$	Rated AC voltage (kV)	220
$I_{AClineWP}$	Rated AC current (kA)	0.775
$R_{AClineWP}$	AC line resistance (Ω/km)	0.001724
$L_{AClineWP}$	AC line inductance (mH/km)	0.4
$C_{AClineWP}$	AC line parallel capacitance (μF/km)	0.22
$l_{AClineWP}$	AC line length (km)	10

Table 10: EMT model parameters of the AC line of the wind park in DIgSILENT PF

B.7 Offshore VSC model (Conv_OFFshore)

Parameter	Description	Value
V_{DC}	Rated DC voltage (kV)	640
V_{AC}	Rated AC voltage (kV)	220
S_{VSC}	Rated VSC power (MVA)	560
R_f	VSC output filter (Ω)	0.001
L_f	VSC output filter(H)	0.014
P_{nold}	No load losses (kW) of VSC	4000
$swtLossFactor$	Switching loss factor (kW/A) of VSC	0
Ron	On resistance for diode/transistor parameter (Ω) of VSC	0.0001
$Goff$	Off-conductance (μS) of VSC	0.001
$R0/R1$	R0/R1 ratio of VSC	1
$X0/X1$	X0/X1 ratio of VSC	1
CapOFFshore	Onshore capacitor (μF)	450

Table 11: EMT model parameters of the offshore VSC model in DIgSILENT PF

B.8 Offshore transformer

Parameter	Description	Value
S_T	Rated apparent power (MVA)	270
f_T	Nominal frequency (Hz)	50
$V_{T,AC,HV}$	Rated voltage-High voltage side (kV)-YN	220
$V_{T,AC,LV}$	Rated voltage-Low voltage side (kV)-Y	66
$X_{1,AC}$	Positive sequence reactance (p.u.)	0.099
$R_{1,AC}$	Positive sequence resistance (p.u.)	0.0011
$C_{AClineWP}$	AC line parallel capacitance (μF/km)	0.22
–	No load current (%)	0.16
–	No load losses (kW)	0

Table 12: Model parameters of offshore transformer in DIgSILENT PF

B.9 Control of offshore VSC

Parameter	Description	Value
k_{AC}	PI constant-AC voltage control	1
T_{AC}	Time constant-AC voltage control	0.01
T_{rudc}	Udc filter time constant	0.01
T_{rac}	Udc filter time constant	0.005
dbd_{udc}	Dead-band udc droop control	0.03
f_{min}	Minimum output frequency-droop control (p.u.)	1
f_{max}	Maximum output frequency-droop control (p.u.)	1.04
udc_{ref}	Voltage setpoint-droop control	1.01
$u_{dc,min}$	Minimum Udc voltage (Droop control) (p.u.)	1
$u_{dc,max}$	Maximum Udc voltage (Droop control) (p.u.)	1.06
$P_{m,min}$	Minimum modulation index (AC voltage control)	0
$P_{m,max}$	Maximum modulation index (AC voltage control)	1

Table 13: Control parameters of offshore VSC in DIgSILENT PF

B.10 Wind farm (WindPark (SG))

Parameter	Description	Value
N_{WT}	Number of wind turbines	100
S_{WT}	Nominal apparent power (MVA)	5.5
pf	Power factor	0.9
P_{WT}	Active power (MW) dispatch for each wind turbine	4
Q_{WT}	Reactive power (MVAr) dispatch for each wind turbine	0

Table 14: Model parameters of offshore wind park in DIgSILENT PF

Appendix C- Parameters of the small signal model

Parameter	Description	Value
V_{DC}	Rated DC voltage (kV)	640
V_{AC}	Rated AC voltage (kV)	275
S_{VSC}	Rated VSC power (MVA)	560
R_f	VSC output filter (Ω)	0.001
L_f	VSC output filter (H)	0.014
R	AC line resistance (Ω/km)	0.015
L	AC line inductance (mH/km)	0.4
C	AC line parallel capacitance (μF/km)	0.22
X/R	AC line X/R ratio	8.37
l_{line}	AC line length (km)	1
ω	Resonant angular frequency -PR control (rad/s)	314.159
k_q	Outer loop control-proportional constant of PI controller in the q axis	0.4
T_q	Outer loop control-time constant of PI controller in the q axis (s)	0.01
k_v	Outer loop control-proportional constant of PI controller in the d axis	30
T_v	Outer loop control-time constant of PI controller in the d axis (s)	0.09
k_{FSM}	Outer loop control-frequency sensitive mode slope	0.05
$k_{droop,AC}$	Outer loop control-droop AC control constant	-2.2
$T_{rV_{DC}}$	Filter time constant-DC voltage (s)	0.01
T_{rq}	Filter time constant -reactive power (s)	0.02
dbd	Dead-band droop AC Voltage (p.u.)	0.005
k_p	Inner loop control-proportional constant of PR controller in dq axis	1.5
k_i	Inner loop control-integral constant of PR controller in dq axis (s)	30000

Table 15: Parameters of the small signal model

References

[1] ABB Technology Ltd (2014). ABB Review Special Report: 60 years of HVDC. [online]. Available: https://library.e.abb.com/public/aff841e25d8986b5c1257d380045703f/140818%20ABB%20SR%2060%20years%20of%20HVDC_72dpi.pdf. Accessed: 2020-04-02.

[2] European Commission-Intelligent Energy Europe (2019). Friends of the supergrid. [online]. Available: https://ec.europa.eu/energy/intelligent/projects/en/partners/fosg. Accessed: 2020-04-02.

[3] ABB Technology Ltd (2020). Québec - New England The first large scale multiterminal HVDC transmission in the world to be upgraded. [online]. Available: https://new.abb.com/systems/hvdc/references/quebec-new-england. Accessed: 2020-04-02.

[4] Terna (2020). Sardinia-corsica-italy interconnection (sa.co.i.3 project). [online]. Available: https://www.terna.it/en/projects/projects-common-interest/sardinia-corsica-italy-interconnection. Accessed: 2020-04-02.

[5] G. Buigues, V. Valverde, A. Etxegarai, P. Eguia, and E. Torres. Present and future multiterminal HVDC systems: current status and forthcoming. In *International Conference on Renewable Energies and Power Quality (ICREPQ'17)*, pages 83–88, Salamanca (Spain), June 2017.

[6] D. Jovcic, L. Lamont, and K. Abbott. Control system design for VSC transmission. *Electric Power Systems Research*, vol. 77:pages 721 – 729, 2007.

[7] A. Lesnicar and R. Marquardt. An innovative modular multilevel converter topology suitable for a wide power range. In *2003 IEEE Bologna Power Tech Conference Proceedings*, volume 3, pages 6 pp. Vol.3–, Bologna (Italy), June 2003.

[8] C. Castillo Bonilla and S. Merilyn Tigga. Master's Thesis: Design and performance comparison of Two-level and Multilevel Converters for HVDC Applications. Master's thesis, Chalmers University of Tehnology, Göteborg, Sweden, 2011.

[9] P. Kundur, J. Paserba, V. Ajjarapu, G. Andersson, A. Bose, C. Canizares, N. Hatziargyriou, D. Hill, A. Stankovic, C. Taylor, T. Van Cutsem,

and V. Vittal. Definition and classification of power system stability IEEE/CIGRE joint task force on stability terms and definitions. *IEEE Transactions on Power Systems*, vol. 19:pages 1387–1401, August 2004.

[10] R. Makaliki. Master's Thesis: Voltage Sag Source Location in Power Systems. Master's thesis, Chalmers University of Tehnology, Göteborg, Sweden, 2006.

[11] S. Papaefthimiou, S. Papathanassiou, and M. Ppapadopoulos. Evaluation of voltage dip characteristics in autonomous island networks and correlation with wind turbine frt curves. In *CIRED 2009 - 20th International Conference and Exhibition on Electricity Distribution - Part 1*, pages 1–4, Prague (Czech Republic), 2009.

[12] I. Egido, F. Fernandez-Bernal, P. Centeno, and L. Rouco. Maximum frequency deviation calculation in small isolated power systems. *IEEE Transactions on Power Systems*, vol. 24(4):pages 1731–1738, September 2009.

[13] E.ON Netz GmbH (2006). Grid code. High and extra high voltage. [online]. Available: `https://www.nerc.com/docs/pc/ivgtf/German_EON_Grid_Code.pdf`. Accessed: 2020-04-02.

[14] E. Robles, M. Haro-Larrode, M. Santos-Mugica, A. Etxegarai, and E. Tedeschi. Comparative analysis of European grid codes relevant to offshore renewable energy installations. *Renewable and Sustainable Energy Reviews*, vol. 102:pages 171–185, March 2019.

[15] A. Egea-Alvarez, S. Fekriasl, F. Hassan, and O. Gomis-Bellmunt. Advanced vector control for voltage source converters connected to weak grids. *IEEE Transactions on Power Systems*, vol. 30(6):pages 3072–3081, November 2015.

[16] J. Freytes, L. Papangelis, H. Saad, P. Rault, T. Van Cutsem, and X. Guillaud. On the modeling of MMC for use in large scale dynamic simulations. In *2016 Power Systems Computation Conference (PSCC)*, pages 1–7, Genoa (Italy), June 2016.

[17] M. Amin, J. A. Suul, S. D'Arco, E. Tedeschi, and M. Molinas. Impact of state-space modelling fidelity on the small-signal dynamics of VSC-HVDC systems. *11th IET International Conference on AC and DC Power Transmission*, February 2015.

[18] Mohammad Amin and Marta Molinas. Small-Signal Stability Assessment of Power Electronics Based Power Systems: A Discussion of Impedance- and Eigenvalue-Based Methods. *IEEE Transactions on Industry Applications*, vol. 53(5):pages 5014–5030, September 2017.

[19] H. Saad, J. Mahseredjian, S. Dennetière, and S. Nguefeu. Interactions studies of HVDC–MMC link embedded in an AC grid. *Electric Power Systems Research*, vol. 138:pages 202–209, September 2016.

[20] G. Pinares. Analysis of the DC dynamics of VSC-HVDC systems connected to weak AC grids using a frequency domain approach. In *2014 Power Systems Computation Conference*, Wroclaw (Poland), August 2014.

[21] O. Kotb, M. Ghandhari, R. Eriksson, and V. Sood. On small signal stability of an AC/DC power system with a hybrid MTDC network. *Electric Power Systems Research*, vol. 136:pages 79–88, July 2016.

[22] P. Lehn and S. Podrucky. Small-signal modeling of power electronic converters with resonant controllers. In *International Conference on Power Systems Transients (IPST)*, Kyoto (Japan), 2009.

[23] R. Teodorescu, F. Blaabjerg, M. Liserre, and P. C. Loh. Proportional-resonant controllers and filters for grid-connected voltage-source converters. *IEE Proceedings - Electric Power Applications*, vol. 153(5):pages 750–762, October 2006.

[24] N. Zhang, H. Tang, and C. Yao. A Systematic Method for Designing a PR Controller and Active Damping of the LCL Filter for Single-Phase Grid-Connected PV Inverters. *Energies*, vol. 7(6):pages 3934–3954, June 2014.

[25] J. Hwang, P. Lehn, and M. Winkelnkemper. A Generalized Class of Stationary Frame-Current Controllers for Grid-Connected AC–DC Converters. *IEEE Transactions on Power Delivery*, vol. 25(4):pages 2742–2751, October 2010.

[26] M. Amin. *Small-signal Stability Characterization of Interaction Phenomena between HVDC System and Wind Farms*. PhD thesis, Faculty of Information Technology and Electrical Engineering, Department of Engineering Cybernetics, Norwegian University of Science and Technology, Trondheim, Norway, June 2017.

[27] D. Lin. Master's Thesis: Methods for Analyzing Power System Small Signal Stability. Master's thesis, Faculty of Engineering and Applied Science, Memorial University of Newfoundland, St. John's Newfoundland and Labrador (Canada), October 2015.

[28] DIgSILENT Power Factory (2020). PowerFactory - DIgSILENT. [online]. Available: `https://www.digsilent.de/en/powerfactory.html`. Accessed: 2020-04-02.

[29] P. Almeida, P. Barbosa, J. Oliveira, J. Duarte, and P. Ribeiro. Digital proportional multi-resonant current controller for improving grid-connected photovoltaic systems. *Renewable Energy*, vol. 76:pages 662–669, April 2015.

[30] Massachusetts Institute of Technology (2003). Department of Electrical Engineering and Computer Science. Lyapunov Methods. [online]. Available: `https://dspace.mit.edu/bitstream/handle/1721.1/74611/6-241-fall-2003/contents/recitations/rec6.pdf`. Accessed: 2020-04-02.

[31] M. Amin, A. Rygg, and M. Molinas. Impedance-based and eigenvalue based stability assessment compared in VSC-HVDC system. In *2016 IEEE Energy Conversion Congress and Exposition (ECCE)*, pages 1–8, Milwaukee, WI, (United States), September 2016.

[32] S. Sanchez, G. Bergna, and E. Tedeschi. Tuning of control loops for grid-connected Modular Multilevel Converters under a simplified port representation for large system studies. In *2017 Twelfth International Conference on Ecological Vehicles and Renewable Energies (EVER)*, pages 1–8, Monte-Carlo, Monaco, April 2017.

[33] D. Chen and K. Ding. Chapter 4 - System Stability and Control Technologies after Large-Scale Wind Power Integration. In *Large-Scale Wind Power Grid Integration*, pages 107 – 184. Academic Press, Oxford, 2016.

[34] Wenjuan Du, Qiang Fu, Xubin Wang, and H. F. Wang. Small-signal stability analysis of integrated VSC-based DC/AC power systems – A review. *International Journal of Electrical Power & Energy Systems*, vol. 103:pages 545–552, December 2018.

[35] W. Du, H. Wang, and S. Bu. *Small-Signal Stability Analysis of Power Systems Integrated with Variable Speed Wind Generators*. Springer International Publishing, 2018.

[36] E. Abulanwar. *Wind power integration into weak power systems*. PhD thesis, Department of Energy Technology, Aalborg University, 2016.

[37] A. Perez Basante. *Modular Multilevel Converters for Medium Voltage Applications: Low Switching Frequency Modulation Strategies and Circulating Current Control Techniques*. PhD thesis, Electronics Technology Department, The University of the Basque Country, 2017.

[38] A. Endegnanew. *Stability Analysis of High Voltage Hybrid AC/DC Power Systems*. PhD thesis, Faculty of Information Technology and Electrical, Department of Electric Power Engineering, Norwegian University of Science and Technology, 2017.

[39] F. Blaabjerg. *Control of Power Electronic Converters and Systems*. Elsevier, Academic Press edition, 2018.

[40] J. Rodriguez, S. Bernet, B. Wu, J. O. Pontt, and S. Kouro. Multilevel Voltage-Source-Converter Topologies for Industrial Medium-Voltage Drives. *IEEE Transactions on Industrial Electronics*, vol. 54(6):pages 2930–2945, December 2007.

[41] S. Rohner, S. Bernet, M. Hiller, and R. Sommer. Modulation, Losses, and Semiconductor Requirements of Modular Multilevel Converters. *IEEE Transactions on Industrial Electronics*, vol. 57(8):pages 2633–2642, August 2010.

[42] H. Alyami and Y. Mohamed. Review and development of mmc employed in vsc-hvdc systems. In *2017 IEEE 30th Canadian Conference on Electrical and Computer Engineering (CCECE)*, pages 1–6, Windsor(Canada), April 2017.

[43] O. Oni, I. Davidson, and K. Mbangula. A review of lcc-hvdc and vsc-hvdc technologies and applications. In *2016 IEEE 16th International Conference on Environment and Electrical Engineering (EEEIC)*, Florence (Italy), June 2016.

[44] A. Aamir, L. Qiao, C. Guo, A. U. Rehman, and Z. Yang. Impact of synchronous condenser on the dynamic behavior of LCC-based UHVDC system hierarchically connected to AC system. *CSEE Journal of Power and Energy Systems*, vol. 5(2):pages 190–198, June 2019.

[45] J. Xu, B. Liu, R. E. Torres-Olguin, and T. Undeland. Grid integration of large offshore wind energy and oil amp; gas installations using lcc hvdc transmission system. In *SPEEDAM 2010*, pages 784–791, June 2010.

[46] Suroso and T. Noguchi. Common-emitter topology of multilevel current-source pulse width modulation inverter with chopper-based dc current sources. *IET Power Electronics*, vol. 4(7):pages 759–766, August 2011.

[47] L. de Oliveira, W. Borges, J. de Souza, and L. Ravagnani. Dc and ac side harmonics in ccc converters. In *2007 IEEE Power Engineering Society Conference and Exposition in Africa - PowerAfrica*, Johannesburg (South Africa), July 2007.

[48] J. Wen, J. Wang, L. Wang, W. Yin, and B. Liu. Evaluation of capacitor commutated converter hvdc for qinghai-xizhang interconnection project. In *9th IET International Conference on AC and DC Power Transmission (ACDC 2010)*, London (United Kingdom), October 2010.

[49] Z. Siyu, W. Jun, C. Wenjia, L. Sizhuo, and Y. Wei-yang. Study on transient characteristics of ccc-hvdc transmission systems. In *International Conference on Sustainable Power Generation and Supply (SUPERGEN 2012)*, Hangzhou (China), September 2012.

[50] N. Flourentzou, V. G. Agelidis, and G. D. Demetriades. Vsc-based hvdc power transmission systems: An overview. *IEEE Transactions on Power Electronics*, vol. 24(3):pages 592–602, March 2009.

[51] G. Ding, G. Tang, Z. He, and M. Ding. New technologies of voltage source converter (vsc) for hvdc transmission system based on vsc. In *2008 IEEE Power and Energy Society General Meeting - Conversion and Delivery of Electrical Energy in the 21st Century*, pages 1–8, Pittsburgh, PA (United States), July 2008.

[52] L. Herrera, X. Yao, and J. Wang. Modeling and circulating current control of mmc. In *2015 IEEE Applied Power Electronics Conference and Exposition (APEC)*, Charlotte, NC, (United States), March 2015.

[53] S. Du, B. Wu, and N. Zargari. Common-mode voltage minimization for grid-tied modular multilevel converter. *IEEE Transactions on Industrial Electronics*, vol. 66(10):pages 7480–7487, October 2019.

[54] X. Yu, J. Yi, N. Wang, Y. Teng, and Q. Huang. Analysis on dynamic response of lcc-vsc hybrid hvdc system with ac/dc faults. In *2018 IEEE Innovative Smart Grid Technologies - Asia (ISGT Asia)*, pages 323–327, Singapore (Singapore), May 2018.

[55] J. Glasdam, J. Hjerrild, Ł. H. Kocewiak, and C. L. Bak. Review on multi-level voltage source converter based hvdc technologies for grid connection of large offshore wind farms. In *2012 IEEE International Conference on Power System Technology (POWERCON)*, pages 1–6, Auckland (New Zealand), October 2012.

[56] ENTSO-E (European Network of Transmission System Operators for Electricity) (2016). Network Code for HVDC Connections and DC-connected Power Park Modules. Explanatory Note. [online]. Available: `https://www.entsoe.eu/network_codes/hvdc/`. Accessed: 2020-04-02.

[57] A. Gavrilovic. Ac/dc system strength as indicated by short circuit ratios. In *International Conference on AC and DC Power Transmission*, London (United Kingdom), September 1991.

[58] J. Gonzalez, C. Weindl, G. Herold, D. Retzmann, H. Cardona, I. Isaac, and G. Lopez. Feasibility of HVDC for Very Weak AC Systems with SCR below 1.5. In *2006 12th International Power Electronics and Motion Control Conference*, pages 1522–1527, Portoroz (Slovenia), August 2006.

[59] O. Nayak, A. Gole, D. Chapman, and J. Davies. Dynamic performance of static and synchronous compensators at an hvdc inverter bus in a very weak ac system. *IEEE Transactions on Power Systems*, vol. 9(3):pages 1350–1358, August 1994.

[60] E. Ebrahimzadeh, F. Blaabjerg, T. Lund, J. Godsk Nielsen, and P. Carne Kjær. Modelling and Stability Analysis of Wind Power Plants Connected to Weak Grids. *Applied Sciences*, vol. 9(21):pages 4695, January 2019.

[61] M. Nawir. *Integration of Wind Farms into Weak AC grids.* PhD thesis, School of Engineering, Cardiff University, Cardiff (United Kindgom), 2017.

[62] L. Zhu, Z. Yuan, C. Sheng, P. Luo, and F. Yang. The Principle and Method of Improving Short Circuit Ratio of LCC-HVDC by VSC-HVDC. *DEStech Transactions on Environment, Energy and Earth Sciences*, February 2018.

[63] PROMOTioN–Progress on Meshed HVDC Offshore Transmission Networks. Deliverable 1.3: Synthesis ofavailable studies on offshore meshed HVDC grids. [online]. Available: https://www.promotion-offshore.net/fileadmin/PDFs/D1.3_PROMOTioN_Deliverable_1.3_Synthesis_of_available_studies.pdf, September 2016.

[64] L. Zhang, L. Harnefors, and H. Nee. Power-Synchronization Control of Grid-Connected Voltage-Source Converters. *IEEE Transactions on Power Systems*, vol. 25(2):pages 809–820, May 2010.

[65] L. Harnefors, M. Bongiorno, and S. Lundberg. Input-Admittance Calculation and Shaping for Controlled Voltage-Source Converters. *IEEE Transactions on Industrial Electronics*, vol. 54(6):pages 3323–3334, December 2007.

[66] P. Mitra, L. Zhang, and L. Harnefors. Offshore wind integration to a weak grid by vsc-hvdc links using power-synchronization control: A case study. *IEEE Transactions on Power Delivery*, vol. 29(1):pages 453–461, February 2014.

[67] R. Geetha, R. Deekshit, and G. Lal. Analysis of vsc-hvdc system connected to a weak ac system. In *2013 Annual IEEE India Conference (INDICON)*, pages 1–6, Mumbai (India), December 2013.

[68] L. Huang, H. Xin, H. Yang, Z. Wang, and H. Xie. Interconnecting very weak ac systems by multiterminal vsc-hvdc links with a unified virtual synchronous control. *IEEE Journal of Emerging and Selected Topics in Power Electronics*, vol. 6(3):pages 1041–1053, September 2018.

[69] A. Etxegarai, P. Eguia, E. Torres, A. Iturregi, and V. Valverde. Review of grid connection requirements for generation assets in weak power grids. *Renewable and Sustainable Energy Reviews*, vol. 41:pages 1501 – 1514, January 2015.

[70] S. Grunau and F. Fuchs. Effect of Wind-Energy Power Injection into Weak Grids. In *European Wind Energy Conference and Exhibition 2012 (EWEC 2012)*, pages 1150–1156, January 2012.

[71] Ipsa Power (2013). A Guide to the DC Decay of Fault Current and X/R Ratios. [online]. Available: https://www.ipsa-power.com/?wpfb_dl=88. Accessed: 2020-04-02.

[72] S. M. Alizadeh, C. Ozansoy, and T. Alpcan. The impact of x/r ratio on voltage stability in a distribution network penetrated by wind farms. In *2016 Australasian Universities Power Engineering Conference (AUPEC)*, pages 1–6, Brisbane, QLD, (Australia), September 2016.

[73] H.R. Najafi, F. Robinson, F. Dastyar, and A.A. Samadi. Transient stability evaluation of wind farms implemented with induction generators. In *2008 43rd International Universities Power Engineering Conference*, pages 1–5, Padova (Italy), September 2008.

[74] S. Tabatabaee, H. R. Karshenas, A. Bakhshai, and P. Jain. Investigation of droop characteristics and x/r ratio on small-signal stability of autonomous microgrid. In *2011 2nd Power Electronics, Drive Systems and Technologies Conference*, pages 223–228, Tehran (Iran), February 2011.

[75] National Grid (2016). The Grid code. Issue 5. Revision 16. [online]. Available: `https://www.nationalgrideso.com/document/34121/download`. Accessed: 2020-04-02.

[76] National Grid (2019). The Grid code. Issue 5. Revision 38. [online]. Available: `https://www.nationalgrideso.com/document/33821/download`. Accessed: 2020-04-02.

[77] Y. Li, S. Yang, K. Wang, and D. Zeng. Research on PI controller tuning for VSC-HVDC system. In *2011 International Conference on Advanced Power System Automation and Protection*, volume 1, pages 261–264, Beijing (China), October 2011.

[78] S. Akkari. *Control of a multi-terminal HVDC (MTDC) system and study of the interactions between the MTDC and the AC grids.* PhD thesis, University Paris-Saclay, 2016.

[79] ALSTOM Grid Worldwide Contact Centre (2020). HVDC for Beginners and Beyond. [online]. Available: `http://cigre.ru/research_commitets/ik_rus/b4_rus/library/ALSTOM_HVDC_for_Beginners_and_Beyond.pdf`. Accessed: 2020-04-02.

[80] A. Egea-Alvarez, J. Beerten, D. Van Hertem, and O. Gomis-Bellmunt. Primary and secondary power control of multiterminal hvdc grids. In *10th IET International Conference on AC and DC Power Transmission (ACDC 2012)*, Birmingham (United Kingdom), December 2012.

[81] S. Nanou, O. Tzortzopoulos, and S. Papathanassiou. Evaluation of dc voltage control strategies for multi-terminal hvdc grids comprising island systems with high res penetration. In *11th IET International Conference on AC and DC Power Transmission*, Birmingham (United Kingdom), February 2015.

[82] S. Wenig, Y. Rink, and T. Leibfried. Multi-terminal hvdc control strategies applied to the cigré b4 dc grid test system. In *2014 49th International Universities Power Engineering Conference (UPEC)*, pages 1–6, Cluj-Napoca (Romania), September 2015.

[83] J. Beerten, S. Cole, and R. Belmans. Modeling of multi-terminal vsc hvdc systems with distributed dc voltage control. *IEEE Transactions on Power Systems*, vol. 29(1):pages 34–42, January 2014.

[84] A. Marten, F. Sass, and D. Westermann. Continuous dc node voltage control characteristic for multi-terminal and meshed hvdc grids. In *2016 IEEE International Energy Conference (ENERGYCON)*, Leuven, (Belgium), April 2016.

[85] F. Fein, J. Borecki, H. Groke, and B. Orlik. Decentral control of multiterminal HVDC systems with automatic exchange of instantaneous and primary reserve power across AC grids. In *2015 17th European Conference on Power Electronics and Applications (EPE'15 ECCE-Europe)*, Geneva (Switzerland), September 2015.

[86] M. Andreasson, R. Wiget, D. V. Dimarogonas, K. H. Johansson, and G. Andersson. Distributed primary frequency control through multiterminal HVDC transmission systems. In *2015 American Control Conference (ACC)*, Chicago, IL (United States), July 2015.

[87] J. Cao, W. Du, H. F. Wang, and S. Q. Bu. Minimization of transmission loss in meshed AC/DC grids with VSC-MTDC networks. *IEEE Transactions on Power Systems*, vol. 28(3):pages 3047–3055.

[88] MARINEL project. Deliverable 2.6. [online]. Available: `http://www.clusterenergia.com/marinel-project`. Accessed: 2020-04-02.

[89] F. Torres, S. Martínez, C. Roa, and E. López. Comparison between voltage droop and voltage margin controllers for mtdc systems. In *2018 IEEE International Conference on Automation/XXIII Congress of the Chilean*

Association of Automatic Control (ICA-ACCA), Concepcion (Chile), October 2018.

[90] F. D. Bianchi and O. Gomis-Bellmunt. Droop control design for multiterminal vsc-hvdc grids based on lmi optimization. In *2011 50th IEEE Conference on Decision and Control and European Control Conference*, Orlando, FL (United States), December 2011.

[91] S. Fragoso Rodrigues. Master's Thesis: Dynamic Modeling and Control of VSC-based Multi-terminal DC Networks. Master's thesis, Universidade Técnica de Lisboa, Lisbon (Portugal), 2011.

[92] Y. Shakweh. 33 - Drives Types and Specifications. In M. Rashid, editor, *Power Electronics Handbook (Third Edition)*, pages 881 – 913. Boston (United States), third edition, 2011.

[93] D. Mondal, A. Chakrabarti, and A. Sengupta. Chapter 2 - fundamental models of synchronous machine. In *Power System Small Signal Stability Analysis and Control*, pages 15 – 40. Academic Press, Boston (United States), 2014.

[94] F. Thams, R. Eriksson, and M. Molinas. Interaction of Droop Control Structures and Its Inherent Effect on the Power Transfer Limits in Multiterminal VSC-HVDC. *IEEE Transactions on Power Delivery*, vol. 32(1):pages 182–192, February 2017.

[95] J. Renedo, A. García-Cerrada, and L. Rouco. Active power control strategies for transient stability enhancement of ac/dc grids with vsc-hvdc multiterminal systems. *IEEE Transactions on Power Systems*, vol. 31(6):pages 4595–4604, November 2016.

[96] B. Silva, C. L. Moreira, and H. Leite. Operation and control of multiterminal hvdc grids following the loss of an onshore converter. In *2013 IEEE PES Conference on Innovative Smart Grid Technologies (ISGT Latin America)*, pages 1–8, Sao Paulo, (Brazil), April 2013.

[97] J. Beerten and R. Belmans. Analysis of power sharing and voltage deviations in droop-controlled dc grids. *IEEE Transactions on Power Systems*, vol. 28(4):pages 4588–4597, November 2013.

[98] G. Bergna-Diaz, J. Suul, and S. D'Arco. Energy-Based State-Space Representation of Modular Multilevel Converters with a Constant Equilibrium

Point in Steady-State Operation. *IEEE Transactions on Power Electronics*, vol. 33(6):pages 4832–4851, June 2018.

[99] D. Zmood and D. Holmes. Stationary frame current regulation of pwm inverters with zero steady state error. In *30th Annual IEEE Power Electronics Specialists Conference*, Charleston, SC (United States of America), August 1999.

[100] F. de Bosio, M. Pastorelli, L. Ribeiro, M. Lima, F. Freijedo, and J. Guerrero. Current control loop design and analysis based on resonant regulators for microgrid applications. In *IECON 2015 - 41st Annual Conference of the IEEE Industrial Electronics Society*, Yokohama, (Japan), November 2015.

[101] T. Ngo and S. Santoso. Improving proportional-resonant controller for unbalanced voltage and frequency variation grid. In *2016 IEEE/PES Transmission and Distribution Conference and Exposition (T D)*, Dallas, TX (United States), May 2016.

[102] UCTE ad hoc group(2008)(Union for the Coordination of the Transmission of Electricity). Frequency quality investigation. Excerpt of final report.

[103] G. Bergna Diaz, J. A. Suul, and S. D'Arco. Small-signal state-space modeling of modular multilevel converters for system stability analysis. In *2015 IEEE Energy Conversion Congress and Exposition (ECCE)*, pages 5822–5829, Montreal, QC (Canada), September 2015.

[104] S. D'Arco, J. A. Suul, and M. Molinas. Implementation and analysis of a control scheme for damping of oscillations in vsc-based hvdc grids. In *2014 16th International Power Electronics and Motion Control Conference and Exposition*, pages 586–593, Antalya (Turkey), September 2014.

[105] M. Zadeh, M. Amin, J. Suul, M. Molinas, and O. Fosso. Small-signal stability study of the cigré dc grid test system with analysis of participation factors and parameter sensitivity of oscillatory modes. In *2014 Power Systems Computation Conference*, pages 1–8, Wroclaw (Poland), August 2014.

[106] G. Li, Z. Du, T. An, Y. Xia, and J. Lei. Impact of PLL and VSC control parameters on the AC/MTDC systems stability. *Electric Power Systems Research*, vol. 141:pages 476 – 486, September 2016.

[107] A. Alsseid, D. Jovcic, and A. Starkey. Small signal modelling and stability analysis of multiterminal vsc-hvdc. In *Proceedings of the 2011 14th European Conference on Power Electronics and Applications (EPE 2011)*, Birmingham (United Kingdom), October 2011.

[108] C. Guo, W. Liu, C. Zhao, and X. Ni. Small-signal dynamics and control parameters optimization of hybrid multi-infeed HVDC system. *International Journal of Electrical Power & Energy Systems*, vol. 98:pages 409–418, June 2018.

[109] G. Pinares, L. Bertling Tjernberg, L. Tuan, C. Breitholtz, and A. Edris. On the analysis of the dc dynamics of multi-terminal vsc-hvdc systems using small signal modeling. In *2013 IEEE Grenoble Conference*, pages 1–6, Grenoble (France), June 2013.

[110] ENTSO-E (European Network of Transmission System Operators for Electricity) (2017). Frequency Sensitive Mode-ENTSO-E guidance document for national implementation for network codes on grid connection. [online]. Available: `https://consultations.entsoe.eu/system-development/entso-e-connection-codes-implementation-guidance-d-4/user_uploads/1---igd-on-fsm.pdf`. Accessed: 2020-04-02.

[111] ENTSO-E (European Network of Transmission System Operators for Electricity) (2013). Network Code for Requirements for Grid Connection Applicable to all Generators (RfG). [online]. Available: `https://rustyb.github.io/ee-bites/network_codes/rfg/`, note = Accessed: 2020-04-02.

[112] G. Bergna, J. A. Suul, and S. D'Arco. Impact on small-signal dynamics of using circulating currents instead of ac-currents to control the dc voltage in mmc hvdc terminals. In *2016 IEEE Energy Conversion Congress and Exposition (ECCE)*, pages 1–8, Milwaukee, WI (United States), September 2016.

[113] M. H. Larrode, Í V. Temez, S. C. Recio, M. S. Mugica, and P. E. Lopez. Integral control of a Multi-Terminal HVDC-VSC transmission system. In *2017 Twelfth International Conference on Ecological Vehicles and Renewable Energies (EVER)*, pages 1–15, Monte-Carlo (Monaco), April 2017.

[114] L. Harnefors. Modeling of three-phase dynamic systems using complex

transfer functions and transfer matrices. *IEEE Transactions on Industrial Electronics*, vol. 54(4):pages 2239–2248, August 2007.

[115] P. Kundur. *Power System Stability and Control.* McGraw-Hill, January 1994.

[116] D. Jovcic and K. Ahmed. *High Voltage Direct Current Transmission. Converters, Systems and DC grids.* John Wiley Sons Ltd, 2015.

[117] J. Machowski, J Bialek, and J Bumby. *Power System Dynamics. Stability and Control.* John Wiley Sons Ltd 2012, January 2012.

[118] R. Eriksson. Coordinated control of multiterminal dc grid power injections for improved rotor-angle stability based on lyapunov theory. *IEEE Transactions on Power Delivery*, vol. 29(4):pages 1789–1797, August 2014.

[119] J. Sun. Impedance-based stability criterion for grid-connected inverters. *IEEE Transactions on Power Electronics*, vol. 26(11):pages 3075–3078, November 2011.

[120] K. Ogata. *Modern control engineering.* Prentice Hall, 4. ed., international ed edition, 2002.